SPACE TELESCOPE SCIENCE INSTITUTE
Operated for NASA by AURA

Instrument Science Report WFPC2 00-02

Results of the WFPC2 Observatory Verification after Servicing Mission 3a

Stefano Casertano, Shireen Gonzaga, Sylvia Baggett, Jesus Balleza, John Biretta, Inge Heyer, Anton M. Koekemoer, Chris O'Dea, Adam Riess, Al B. Schultz, and Michael S. Wiggs

July 17, 2000

ABSTRACT

After six weeks of inactivity, the Servicing Mission 3a, and the tests and observations carried out as part of the ensuing Observatory Verification phase, WFPC2 restarted science operations on January 12, 2000. Our calibrations show that the camera remains essentially unchanged with respect to pre-SM3a operations. Other than minor changes due to normal aging of the camera, the only discernible effect of the Servicing Mission was the expected increase, significant but temporary, in the rate at which UV-opaque contaminants collect onto the CCD windows.

1: Introduction

The Wide Field and Planetary Camera 2 (WFPC2) is a two-dimensional imaging photometer utilizing four charge coupled devices (CCDs) as detectors. WFPC2 is located at the center of the Hubble Space Telescope (HST) focal plane, and the WFPC2 field-of-view (FOV) is divided into four CCD cameras (PC, WF2, WF3, WF4) by a four-faceted pyramid mirror near the HST focal plane. Each of the four cameras contains an 800x800 pixel Loral CCD detector.

HST entered Zero Gyro Safe mode at 8:30 AM, November 13, 1999. Entry into safe mode was nominal. The HST aperture door closed during safe mode entry and remained closed until the end of HST Servicing Mission 3a (SM3a). Following entry of HST into

safe mode, WFPC2 was safed. The power to the replacement heaters was kept on, while the power to the detectors, to the computer, and to the mechanisms was turned off. WFPC2 was placed in “protect safe” mode (heat pipe heater on, F785LP filter in, shutter closed) at 9:50 pm on December 22, 1999; in this state, enough power was turned on to keep WFPC2 warm and to make sure telemetry was received for monitoring of the instrument. HST was released by the shuttle crew at 6:03 PM, December 25, 1999. The aperture door was opened for the first time in 42 days, starting the Servicing Mission Observatory Verification 3a (SMOV3a) which verified the correct functioning of HST and its instruments and recommissioned them for normal operations.

The recommissioning of the Wide Field and Planetary Camera 2 took place through a carefully planned sequence of operations, observations and verifications. WFPC2 was recovered from Protect Safe mode to Standby at 2:00 pm on December 27, 1999. An engineering matrix verification plan was carried out to ensure nominal instrumental functionality. Calibration observations then verified that the camera performance and characteristics were essentially the same as before, despite the long period of inactivity following the safing, and the camera resumed science observations on January 12, 2000. This Report documents the WFPC2 observations associated with the SMOV3a, as well as the analysis carried out by the WFPC2 group to validate the camera performance.

Plan

The recommissioning of WFPC2 and verification of its performance and calibration closely followed the plans laid out in the Instrument Science Report WFPC2 99-03, with minor deviations and additions which will be identified where appropriate.

A major concern for WFPC2 is UV-obscuring contamination, especially since contaminating substances condense preferentially on the cold (-88 C) camera heads and progressively reduce the UV throughput of the camera. During normal operations, the total throughput at 170 nm decreases by about 0.6% per day, and the camera heads are warmed every 4 weeks to evaporate contaminants and restore the UV throughput. The rate of accumulation of contaminants increases immediately after servicing missions, and the recommissioning program after Servicing Mission 3a was designed to verify that the total contamination would never exceed the safe level of 30% at 170 nm.

Another contamination concern is the possibility of depositing a very thin layer of contaminants on the optical surfaces exposed to the HST hub area, especially the WFPC2 pick-off mirror. This concern arises from the experience with WF/PC1, whose pick-off mirror eventually lost almost all its reflectivity at the shortest wavelengths. The effect of thin layer contamination is very wavelength-dependent, and is especially noticeable at Lyman α (122 nm). Once deposited, such thin layers of contaminants might evaporate again over time, unless polymerized by strong UV radiation - such as could be caused by Earth light shining inside the mirror. Therefore HST was constrained not to point at the illuminated Earth at any time within the first 12 days after the Servicing Mission (the so-

called period of Bright Earth Avoidance, or BEA), and the end of BEA was tied to verification of the absence of significant far-UV contamination.

Other activities carried out during the WFPC2 Servicing Mission 3a Observatory Verification (SMOV 3a) program included measurements of the HST focus position - with the possibility of refocusing if necessary - as well as verification of the WFPC2 flat field, dark current, bias level, point-spread function (PSF), and photometric throughput. The programs used to carry out all these activities are listed in Table 1.1.

Organization of this Report

The remainder of the present report is divided into seven Sections, each corresponding to a different area of activity and verification. The Sections are listed in Table 1.1. In the interest of efficiency, each of these areas has been addressed by a different subset of the WFPC2 group. The respective authors are identified in each Section. Separate reports have also been released on Lyman α contamination (WFPC2 TIR 00-02, Baggett and Heyer), Photometric throughput (WFPC2 TIR 00-03, Schultz et al), Camera internals (WFPC2 TIR 00-04, O'Dea et al), and Flat field (WFPC2 TIR 00-01, Koekemoer et al.).

Table 1.1: WFPC2 Calibration and Verification Programs for SMOV3a

Section	Title	Program ID	Page
2	Recovery and observations at -57 C	8491	3
3	UV contamination monitoring at the standard operating temperature	8491, 8492	7
4	Lyman α contamination	8491, 8494	12
5	Photometric throughput	8496	19
6	Point spread function	8497	30
7	Camera internals	8491, 8498	31
8	Flat field	8495	46
-	Pre-SM3a baseline observations	8515	-

2: Recovery and Observations at -57 C

by Stefano Casertano, Shireen Gonzaga, and Sylvia Baggett

Summary: Before bringing WFPC2 back to its normal operating temperature of -88 C, it was kept for two days at -57 C and the contamination measured. Since no drop of the UV throughput was observed, with an upper limit of 1%, we were able to proceed with the default plan, and bring the camera to its normal operating temperature.

As the first step in the WFPC2 cooldown procedure, the camera heads were cooled to an intermediate temperature around -57 C for two days. The actual temperature was -55 C for the PC camera head, -57 C for WF2 and WF3, and -58 for WF4. Contamination monitoring observations were taken at 24 hour intervals in all four chips through the filter F170W, to verify whether any contamination was present. Under normal circumstances, no contamination is expected at -57 C; any anomalous contamination at the level of 1% or more might be indicative of the presence of high molecular weight contaminants which could become dangerous at the standard operating temperature of -88 C.

The cooldown and measurement process consisted of four separate steps:

1. Execute transition from the Protect Safe Mode in which WFPC2 was left at the end of the servicing mission (shutter closed, TECs off, F785LP in the optical path) to Hold Mode
2. Execute a 16-hour Protect Decontamination procedure (heaters on, detectors at +22 C, shutter closed, F785LP in optical path)
3. Cool down to -57 C; take observations of BEA UV-bright standard at approximate 24-hour intervals (three epochs)
4. Execute a 24-hour Protect Decontamination to remove any accumulated contaminants while the data are analyzed.

In order to accommodate the possibility of anomalous contamination, a schedule break opportunity was created at the end of the final 24-hour decontamination, and a contingency path devised. In the event of anomalous contamination, the camera would be kept in the warm (decontamination) state as long as required, and the same cooldown procedure, with contamination monitor, would be executed again when deemed safe.

The procedure executed as planned, and we detected no contamination at -57 C at the threshold level of 1%. Therefore we were able to continue with the default plan of cooling down to -88 C and beginning normal WFPC2 operations.

Photometry at -57 C

The photometric procedure employed for the -57 C data was modified with respect to the standard photometry used for calibration data. With the detectors at -57 C, the dark current is substantially higher (about a factor 20) than at -88 C, and the background is thus elevated. In addition, the effect of the numerous hot pixels in the WFPC2 detectors has to be taken into account. Normally, hot pixels have a small impact for bright sources in short exposures and can be identified and rejected without difficulty. At -57 C, hot pixels are a significant contributor to the total signal even for a bright source in a short exposure.

The effect of hot pixels is to skew the distribution of noise in the background, introducing a tail at high signal level. The photometric signal is summed over the chosen aperture, thus hot pixels within the aperture contribute to the signal. On the other hand,

normal background determination is geared to the center of the distribution of background pixels, and does not take the long tail into account. We tried several methods to compute the background, and none gave satisfactory results.

Figure 2.1: Measured counts for the BEA UV-bright standard WD 0710+741 at -57 C. Each point is the average of two measurements; vertical bars indicate the range of the measurements. The dashed line and open symbol for WF4 on Day 3 includes the anomalous high point; the solid line and filled symbol excludes it, and is based on a single measurement.

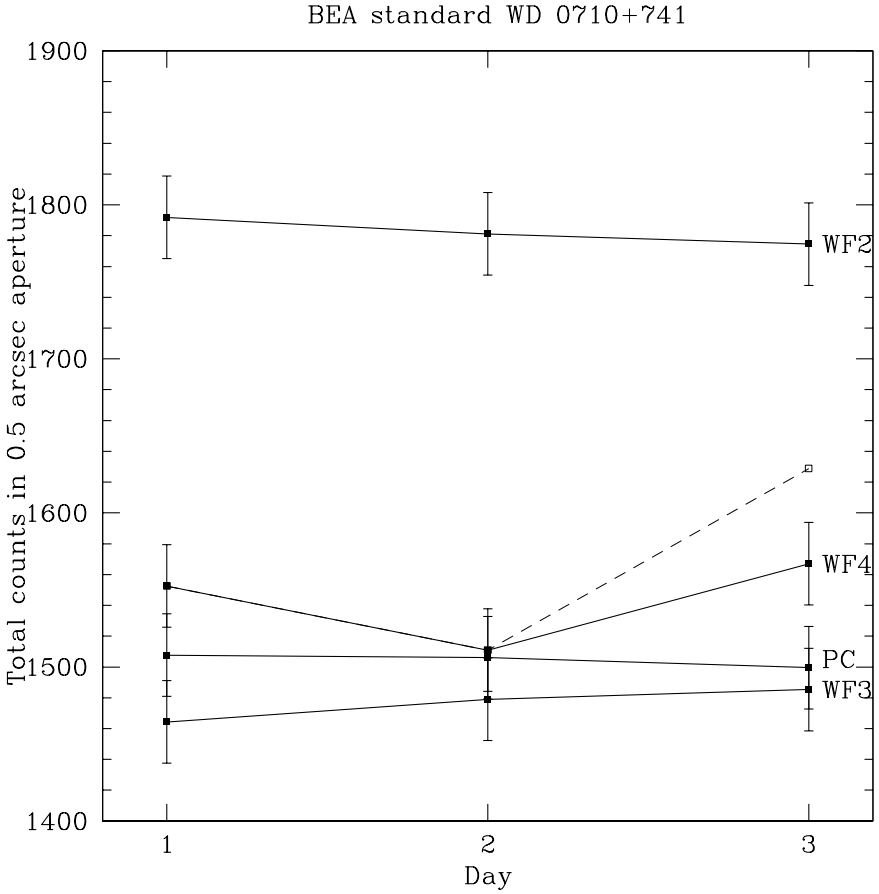

We therefore resorted to determining the background with the classic growth curve technique: the background was adjusted so that the total signal would converge to a well-defined value. We used an outer radius of 50 pixels. This method was very successful, as the photometry obtained with the background thus determined produced well-behaved results.

Results

The photometric measurements for each detector and epoch are shown in Figure 2.1. Since we have little information on the absolute photometric sensitivity of the detectors at -57 C, the photometric results were used exclusively in a relative sense. The photometry

points are the average of two measurements for each detector at each epoch. Most measurements are extremely consistent with one another, but there was one anomalous high point (about 8% high) in WF4 on the third day. We found no obvious reason for the high point, and we performed the analysis with and without it.

Figure 2.2: Relative photometry at -57 C. All measurements are scaled to the mean for each detector, and averaged together. The dashed line includes the anomalous point in WF4. Vertiocal bars indicate the rms variation. Daily averages deviate less than 0.3% from the overall average; the deviation is 1% if the anomalous point is included.

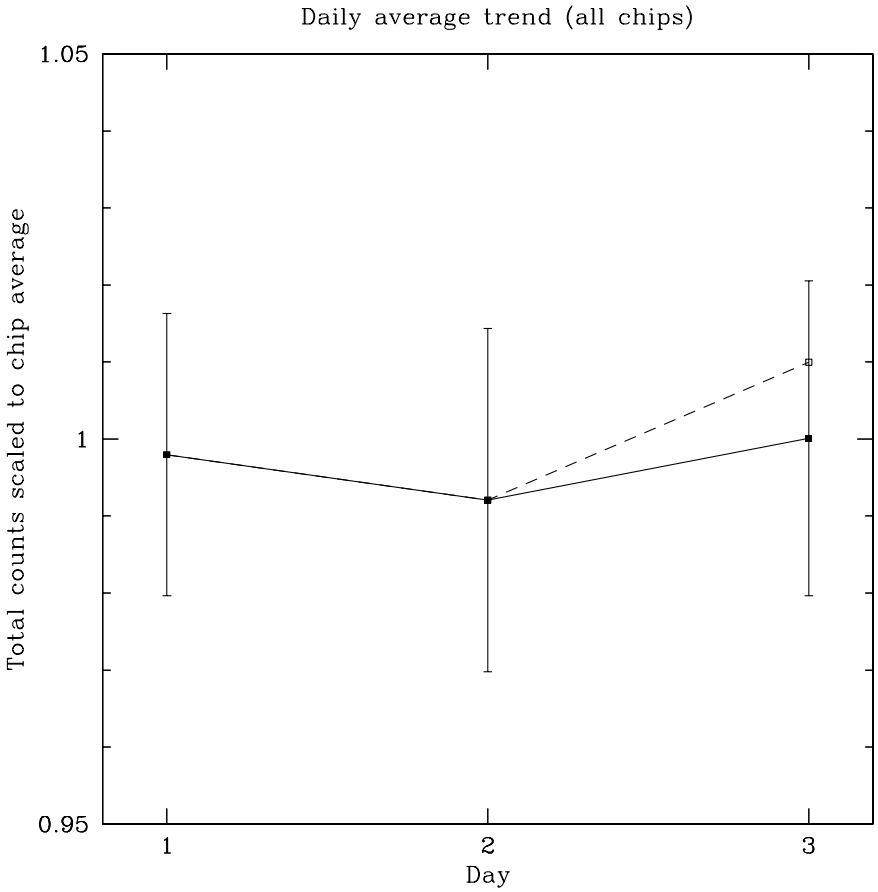

With the exception of the anomalous high point, individual measurements for each detector are all within 3% of the mean value for that detector. We scaled each measurement to the overall average for that detector, and averaged all four detectors together; the resulting points are shown in Figure 2.2. Without the anomalous point, daily averages are all within 0.3% of the overall average; with the anomalous point, the maximum deviation is 1%. In either case, there is absolutely no evidence of a decline in throughput at better than 1% accuracy. Therefore we concluded that there was no safety risk in cooling down WFPC2 to -88 C, and the standard program could proceed.

3: UV contamination monitoring at the standard operating temperature

by Stefano Casertano, Shireen Gonzaga, and Sylvia Baggett

Summary: The UV contamination was monitored constantly during SMOV operations, to ensure that the accumulated contamination would never exceed the WFPC2 safety margin, defined as a throughput drop of 30% at F170W. As was the case after SM2, the contamination rate was significantly higher immediately after servicing, up to 2.5 times the normal rate. However, the accumulated contamination always remained below this safety margin.

The UV contamination monitoring plan for WFPC2 was based on observations of UV standards through the filter F170W, which is also the primary filter for contamination monitoring during normal operations. The program had two phases: an intensive period, starting at the initial cooldown to -88 C and lasting 8 days, and a maintenance period, covering the following 6 weeks. The intensive period coincided with the planned BEA period, and used the BEA UV standard WD 0710+741; the maintenance period began after BEA, and used the primary WFPC2 standard GRW +70d5824. The observations were used to monitor the growth of UV contamination throughout SMOV, and ensure that the projected contamination always remained well within the safety limit, which for WFPC2 is defined as a 30% drop in throughput at F170W.

During the intensive period, observations were planned in all four detectors at intervals of 0, 3, 6, 12, 18, 24, 36, 48 hours, 3, 4, 5, and 8 days after the initial cooldown to -88 C. The timing of the actual observations was altered slightly with respect to the original plan because of scheduling constraints, but all observations were executed in agreement with the requirements of the program. All data were reduced and analyzed very quickly, maintaining a total turnaround time well within the 12 hour requirement, and showed that the contamination was always well within the safety margin.

During the maintenance period, observations were obtained once every week, before and after each decontamination, and were used to follow the return of the contamination rate, expected to be higher than normal following a Servicing Mission, to its normal value.

Measurements and procedures

Normal photometric procedures were employed throughout. The data were reduced through the normal pipeline, cosmic rays and other blemishes identified by hand and excluded, and aperture photometry obtained in the standard 0.5 arcsec radius. The data points were collected in a database, and processed after each new observation to determine the contamination growth rate and its error.

Figure 3.1: The individual data points for the UV contamination monitor, scaled to the average of the first three epochs for each detector. The lines indicate the best-fitting linear regression, with the corresponding slope and residual rms given in each panel.

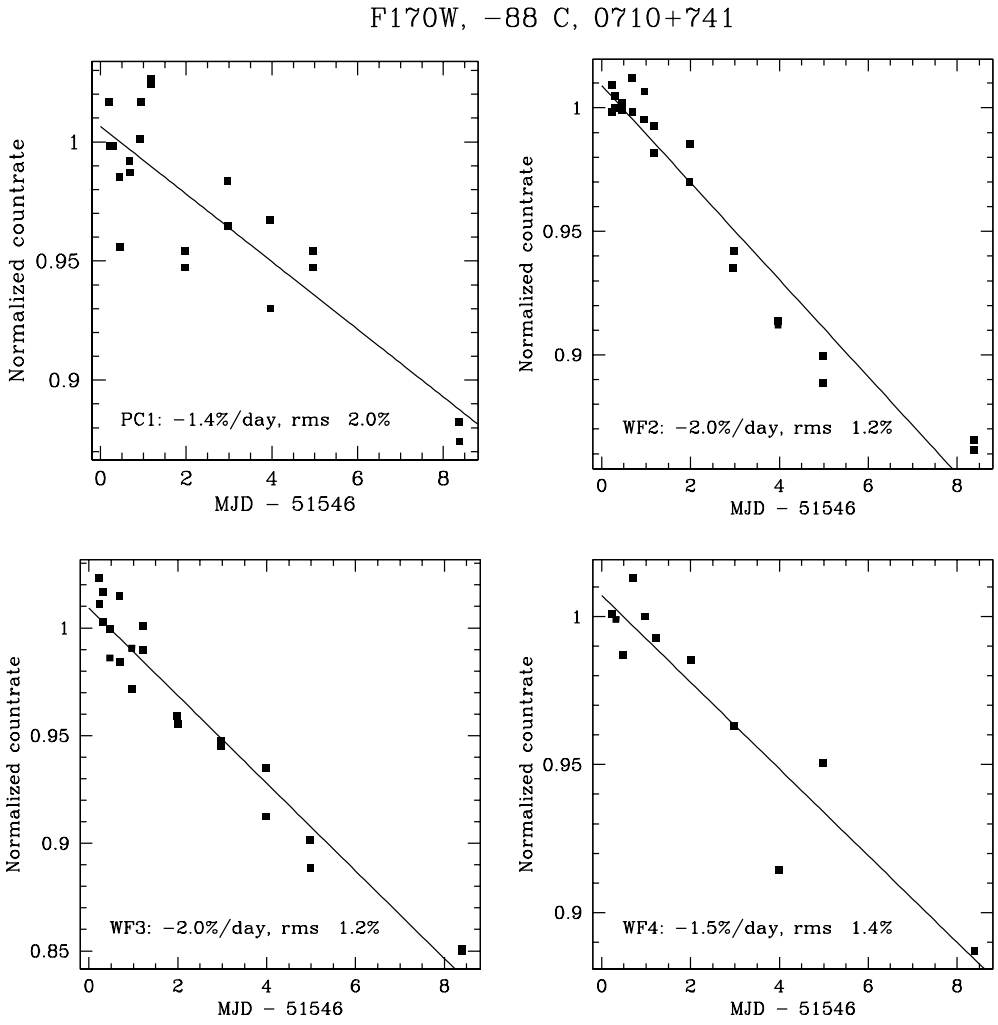

During the intensive monitoring period, data were processed within 12 hours (usually much sooner), and an alert would be raised if at any time the instantaneous contamination rate indicated the possibility of approaching a dangerous level of contamination before the next set of measurements. No alerts occurred; however, at one time, after the 18 hour point, a negative deviation (well within statistical possibility) led to an overestimate of the instantaneous contamination rate and a pre-alert state. The subsequent set of measurements were within the expected range, demonstrating that the event was in fact a statistical fluke, and there was no problem with the WFPC2 contamination.

Results

Figure 3.1 shows the data points obtained for each detector during the intensive monitoring period. Each measurement is rescaled to a fiducial value, consisting of the average for the first three epochs for that detector; the first few points are thus generally above unity. The growth of UV contamination is obvious in the downward trend for all detectors. The slope of each set of points measures the UV contamination rate, which averages between 1.5% and 2%/day throughout this 8-day period. Figure 3.2 shows the combined decline for all four detectors, which is the quantity we compare against the contamination requirement. Since the following decontamination was planned at 12 days after cooldown, the observed contamination rate of 1.8%/day projected to 22% at decontamination, well below the maximum allowable of 30%. Thus the decontamination proceeded as planned and no contingency plan was invoked.

Figure 3.2: Same as Figure 3.1, but with all detectors shown in the same panel and a single regression fitted to all. The mean contamination rate during the first 8 days after cooldown was 1.8% per day (solid line).

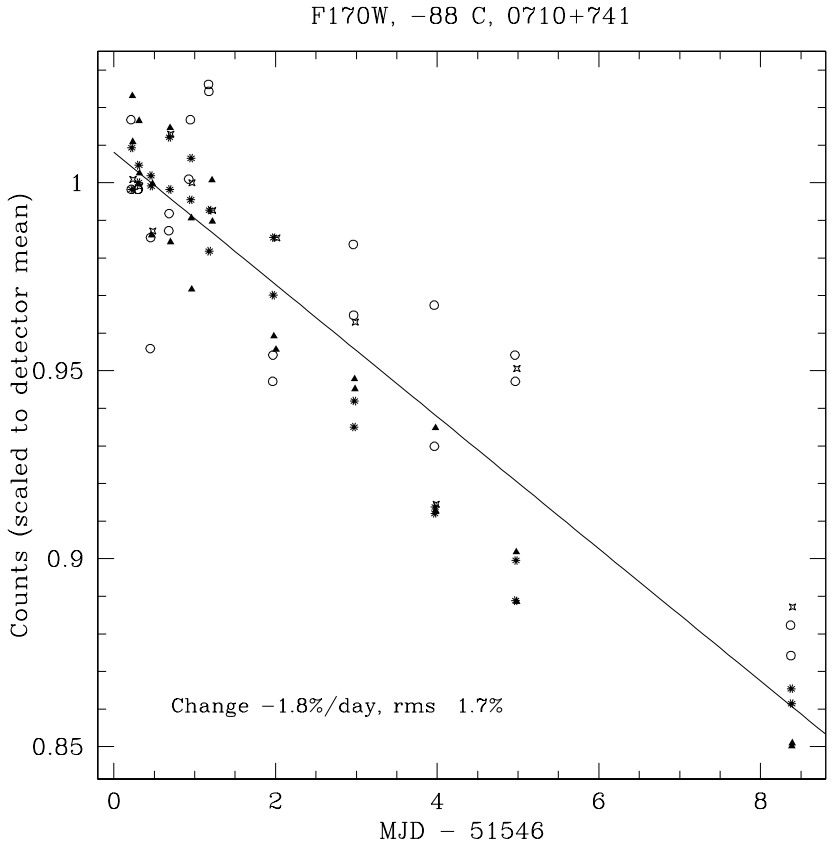

Note that the different contamination rate among detectors is a well-known characteristic of WFPC2. Normal contamination rates in the 1997-98 period (see Table 3.1) are

higher in WF2 and WF3 than in the other two detectors, precisely the same trend seen during SMOV3a.

As in SM2, the contamination rates observed in SMOV3a are substantially higher than normal - about a factor 2.5-3 higher than the 1997-1998 reference values (Table 3.1) - presumably as a consequence of astronauts' activities around the spacecraft and of the installation of new instrumentation. As shown in Table 3.2, the increase in contamination rates has been short-lived. Verification data taken on January 17, January 31, and February 25, each time before and after a decontamination, illustrate the quick return to more normal contamination rates: 1.2%/day on January 17, 0.94%/day on January 31, and 0.78%/day on February 25. The current contamination rate is about 0.5%/day, lower in fact than the 1997-1998 values, as a consequence of the secular decrease in WFPC2 contamination rates.

Table 3.1: F170 contamination rates (percent/day) in early SMOV3a vs. normal rates.

Camera	SMOV3a rate	Normal rate (1997-98)	Ratio (SMOV3a/ normal)	SMOV2 rate
PC	1.4	0.45	3.1	0.82
WF2	2.0	0.80	2.5	1.28
WF3	2.0	0.77	2.6	1.24
WF4	1.5	0.64	2.3	1.04

Table 3.2:F170W contamination rates (percent/day) at various times after SM3a.

MJD start	MJD end	PC	WF2	WF3	WF4
51546.066	51560.684	1.08	1.51	1.41	1.10
51560.684	51574.660	0.84	1.05	1.00	0.88
51574.660	51626.203	0.60	0.90	0.89	0.81
51626.203	51652.820	0.42	0.81	0.80	0.61
51652.820	51709.434	0.35	0.56	0.54	0.51

The contamination rates measured in SMOV3a are significantly higher than in SMOV2, as shown in Table 3.1. However, as Figure 3.3 illustrates, most of the difference is due to the fact that contamination measurements were made earlier in SMOV3a than in SMOV2, 7 to 13 days after release vs. about 18 days for SMOV2. SMOV3a contamination rates are slightly higher than SMOV2 rates ~ 20 days after HST release (average 1.3%/day vs. 1.1%/day), but decrease somewhat faster thereafter, to become comparable 60 days after release and slightly smaller ~ 100 days after release. The overall behavior of the con-

tamination curves and their amplitudes are very similar, and thus there is no evidence for a significant change in the contamination behavior of the telescope. However, the high rates of contamination growth observed soon after HST release suggest that either a shorter interval between decontaminations or a longer wait before WFPC2 cooldown may be desirable in future servicing missions.

Figure 3.3: Contamination rate vs. time since HST release after SM2 and SM3a. The post-SM3a contamination rates are higher, in part because measurements were taken at earlier dates.

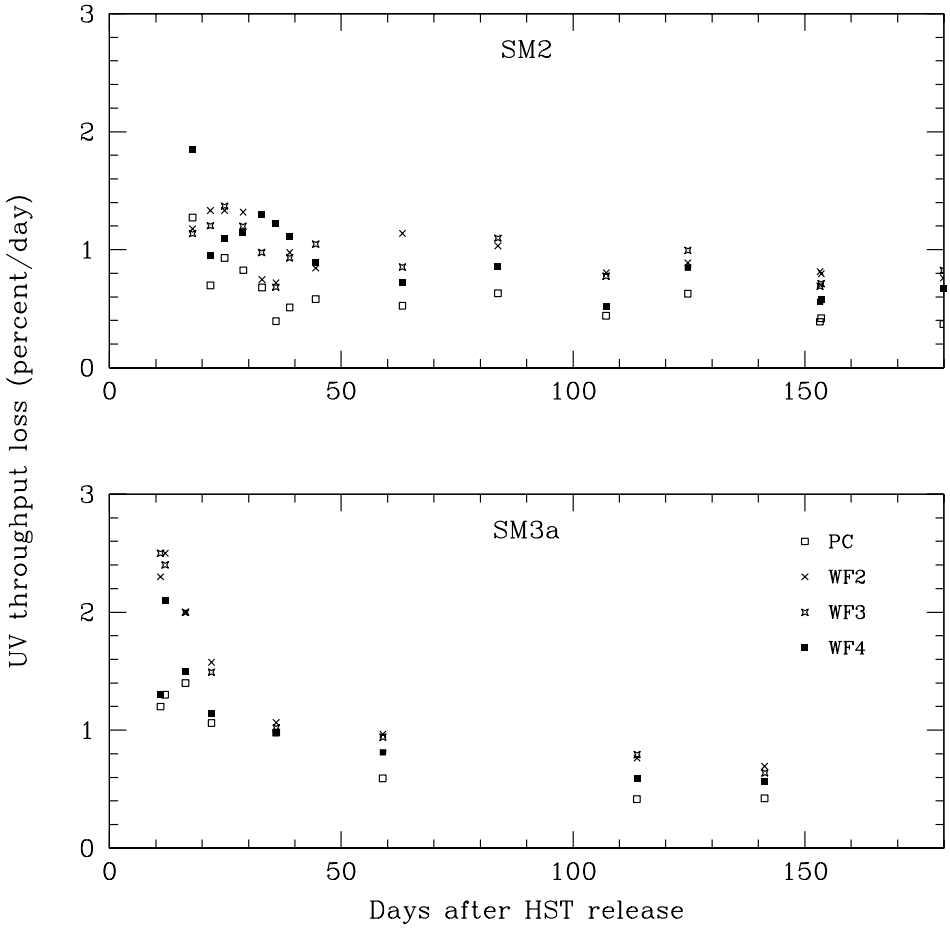

4: Lyman α contamination

by Sylvia Baggett and Inge Heyer

Summary: The far-UV throughput of WFPC2 was monitored during December 1999 and January 2000 for any signs of unexpected throughput degradation following Servicing Mission 3a. No significant changes were detected.
Note: These results have been released independently as WFPC2 Technical Instrument Report (TIR) 00-02, *Results of the WFPC2 SM3a Lyman-α Throughput Check*, by Sylvia Baggett and Inge Heyer.

Introduction

A major concern for WFPC2 during any servicing mission is the possibility of contamination due to the servicing activities. For this reason, SMOV activities for WFPC2 include a variety of controls and checks for contamination, such as special decontamination (decon) sequences, stepped cooldown procedures, intensive photometric monitoring, and contingency planning. The CCD windows can, of course, be heated to remove any contaminant buildup; this is routinely and successfully accomplished with decon procedures about once a month during normal science operations. However, during a servicing mission, contaminants could potentially settle on the pick-off mirror (POM) which is exposed in HST's hub area and cannot be heated. Such contaminants would presumably evaporate over time, but there is the possibility that bright near-UV light, such as that emitted by the illuminated Earth surface, might cause them to polymerize and permanently reduce the sensitivity of HST in the far UV. Therefore, during early SMOV (the BEA, or Bright Earth Avoidance epoch) HST is required to point away from the illuminated Earth surface. The BEA restriction is lifted after observations show normal throughput in the far UV (160 nm and shorter). The Lyman-α throughput tests, based upon observations taken with F160BW and F122M filters, are designed to monitor the far-UV throughput for any signs of degradation which may be due to a layer of contaminants on the pickoff mirror or other exposed surfaces.

During WFPC2's first year in orbit, the stability of the Lyman-α throughput was carefully monitored (MacKenty & Baggett, 1996). The throughput was found to be stable, with an uncertainty of 10 to 20%. Contrasted with the near total loss of Lyman-α reflectivity of the WF/PC-1's pickoff mirror (POM) during its stay in orbit, this suggested that the WFPC2 POM is not likely to develop the same problem unless a new source of contamination is introduced during future servicing missions. Additional Lyman-α monitoring was also done during SMOV2; no significant change in throughput was detected to within the 20% uncertainty (O'Dea et al., 1997). This report presents the Lyman-α monitoring results for SMOV3a.

Data

GRW+70D5824 is the preferred standard photometric monitoring target for WFPC2 and has been routinely used for monitoring observations since early 1994. However, due to BEA restrictions, which call for the avoidance of the bright Earth limb in early SMOV to protect the instruments from excessive UV flux, the GRW+70D5824 pointing was not permitted between Jan 3 and Jan 18, 2000. During this time period, the white dwarf star WD0710+741 served as an alternate standard; since this target had not been previously observed with WFPC2, pre-SMOV3a baseline measurements were taken in October 1999. The properties of the two stars are summarized in Table 4.1.

Table 4.1: Targets used for Lyman-α Throughput Monitoring[a]

Property	Target	
	WD 0710+741	**GRW+70D5824**
RA (J2000.0)	07:17:02.41	13:38:51.77
DEC (J2000.0)	74:00:42.52	70:17:08.5
spectral class	DA2	DA3
V	14.97	12.77
B-V	-0.06	-0.09
U-B	-0.75	-0.84
average count rate F122M	2.9 dn/sec	28.1 dn/sec
observed redleak fraction in F122M	61%	60%
predicted redleak fraction (SYNPHOT)	--	65%
average count rate F160BW	8.4 dn/sec	78.9 dn/sec
observed redleak fraction in F160BW	73%	65%
predicted redleak fraction (SYNPHOT)	--	75%

a. Positions, spectral class, and UBV information for WD 0710+741 and GRW+70D5824 from McCook & Sion (1987) and Turnshek et al. (1990), respectively. Average count rates are at -88 C.

The initial cooldown of the WFPC2 cameras during SMOV3a was performed in two steps: cooling to -57 C followed by a suite of monitoring observations, then, contingent upon nominal results from those observations, cooling to the normal operating temperature of -88 C (Casertano et al., 1999). The Lyman-α observations were obtained at several epochs: pre-SMOV3a (baseline), SMOV3a at -57 C, and finally, SMOV3a at -88 C. For GRW+70D5824, the most recent complete set of far-UV throughput data crossed with F130LP prior to December 1999 are the November 1996 observations, which were taken 3 days after a decon. As discussed in more detail later, we also normalized the F160BW

SMOV3a data to some more recent measurements (August 1997, no F122M data available). The baseline images for WD 0710+741 were taken in October 1999, unfortunately 26 days after a decontamination due to a scheduling error. An estimated contamination correction (0.6%/day, based on long-term F160BW photometric monitoring from Baggett & Gonzaga, 1998) was applied to the baseline data before using them to normalize the SMOV3a data. No contamination rates are available for F122M, so the F160BW correction was applied.

Table 4.2: Timeline of F160BW and F122M Observations[a]

target	date	MJD	proposal	comment
GRW+70D5824	Nov 15, 1996 4:13PM	50402.676	7211	baseline set, 3 days after decon
	Aug 25,1997 07:40AM	50685.32	6936	alternate baseline, ~5 days after decon
	Dec 29, 1999 5:49AM	51541.242	8492	cameras warm (-57 C)
	Dec 29, 1999 12:27PM	51541.519	8492	cameras warm (-57 C)
	Dec 29, 1999 5:04PM	51541.711	8492	cameras warm (-57 C)
	Jan 18 2000 9:32PM	51561.897	8494	cameras at -88 C
WD 0710+741	Oct 4,1999 8:13PM	51455.842	8515	baseline set, 26 days after decon
	Dec 29,1999 9:41AM	51541.403	8492	cameras warm (-57 C)
	Dec 29, 1999 2:18PM	51541.596	8492	cameras warm (-57 C)
	Dec 29, 1999 7:07PM	51541.797	8492	cameras warm (-57 C)
	Jan 3 2000 8:37AM	51546.359	8492	cameras at -88 C
	Jan 3 2000 1:05PM	51546.545	8492	
	Jan 3 2000 5:56PM	51546.747	8492	

a. Date marks start time of observation set. Each set contains a pair of images in each filter combination except for Aug 1997, when only 1 image each of F160BW and F160BW+F130LP were taken (no images in F122M).

The images for the Lyman-α throughput check were taken with the far-UV filters F122M and F160BW: images were taken in single filters as well as crossed with the long-pass filter F130LP to provide an estimate of the redleak correction. Two images were taken with each of the four filter combinations. Due to scheduling restrictions during SMOV3a, only PC was observed in all filter combinations; during SMOV3a, WF3 was used only with the crossed filter configurations and has not been included in this study. Table 4.2 summarizes the observation timeline.

The images were calibrated using the standard STSDAS calwp2 task. The pre-SMOV dark reference files were used to correct for dark current in images taken after the cooldown to the normal operating temperature of -88 C. During the -57 C time period, when the dark current was expected to be 20-60 times higher than normal, no dark correc-

tion was applied; instead, the sky correction in the photometric reductions was relied upon to remove much of the dark level. Disregarding the dark at -57 C appeared to work adequately for GRW+70D5824 but the WD 0710+741 data at that temperature were unusable, due to the lower exposure levels (target is much fainter, see Table 4.1) and the large amount of dark current at -57 C. The analysis of the -57 C WD 0710+741 data was postponed until an approximate dark reference could be generated from five contemporaneous dark frames taken at -57 C.

The flatfields used were the pre-SMOV3a pipeline flats for F122M and F160BW (i5515213u and i5515214u, respectively). Flatfields are not available for the crossed filter combinations so the flatfields for the uncrossed filter were used. Finally, since the flat for F160BW is known to be somewhat noisy (~20% RMS in PC, see, e.g., STAN 33, Aug. 1998), we tried using a sigma-clipped version of the flatfield. One set of images for each target was reduced using the pipeline flat and using the clipped flat; since the resulting photometry differed by less than 0.5%, all SMOV3a data were processed with the standard pipeline flatfield.

After calibration, cosmic rays and hot pixels within the region of interest were removed manually with the IRAF **imedit** task; typically, 4-20 edits were necessary. Centering of the stars was done with the **imcntr** task and refined manually for cases where the PSF was very asymmetric. Photometry was obtained using the STSDAS **digiphot.apphot phot** task, with aperture radius of 0.5” (5 pixels in WF chips, 11 pixels in PC) and sky subtraction annulus from 1.4”-1.9”. The pairs of observations were reduced and analyzed individually; an approximate redleak correction was obtained by subtracting the crossed filter images from the uncrossed filter images. To check repeatability, some datasets were reduced and analyzed by both authors individually; for the final analysis, results from the same person are used although the second set of results are included in the WD 0710+741 plots as small dots.

Results

The normalized count rate ratios are presented in Figure 4.1 and Figure 4.2 for WD 0710+741 and GRW+70d5824, respectively. The final redleak-corrected values are presented. For completeness, the results of the individual observations are included as well.

Each figure illustrates the results from F122M (top row of plots) and F160BW (bottom row of plots). Left most plots show the redleak-corrected normalized count rates, middle plots the normalized count rates for the single filter images, and right most plots the normalized count rates for the crossed filter images. The dashed line marks the date of the cooldown to -88 C. As mentioned earlier, the images were taken in pairs. In Figure 4.1 and Figure 4.2, the middle and right plots (containing crosses) are the results from individual images while the left plots (containing circles) represent the redleak-corrected value for each pair of images (the average of the crossed filter count rates subtracted from the average of the single filter count rates). The small symbols (dots) in Figure 4.1 are independent

measurements of some of the same data presented by the large symbols (circles and crosses), to test repeatability. The independent measurements were found to agree to within at least 10% and usually better than that; the difference was attributed to variations in the cosmic-ray and hot pixel manual editing.

Figure 4.1: SMOV3a Lyman-α throughput check results for WD 0710+741. Top row of plots are for F122M, bottom row plots are for F160BW. Plots from left to right are the normalized count rates for: redleak-corrected, single filter, and crossed filter data as a function of Modified Julian date. Count rates were normalized to the contamination-corrected October 1999 measurements; dashed line marks the date of the SMOV3a cooldown from -57 C to -88 C. The smallest dots are independent measurements of some of the data represented by the large symbols.

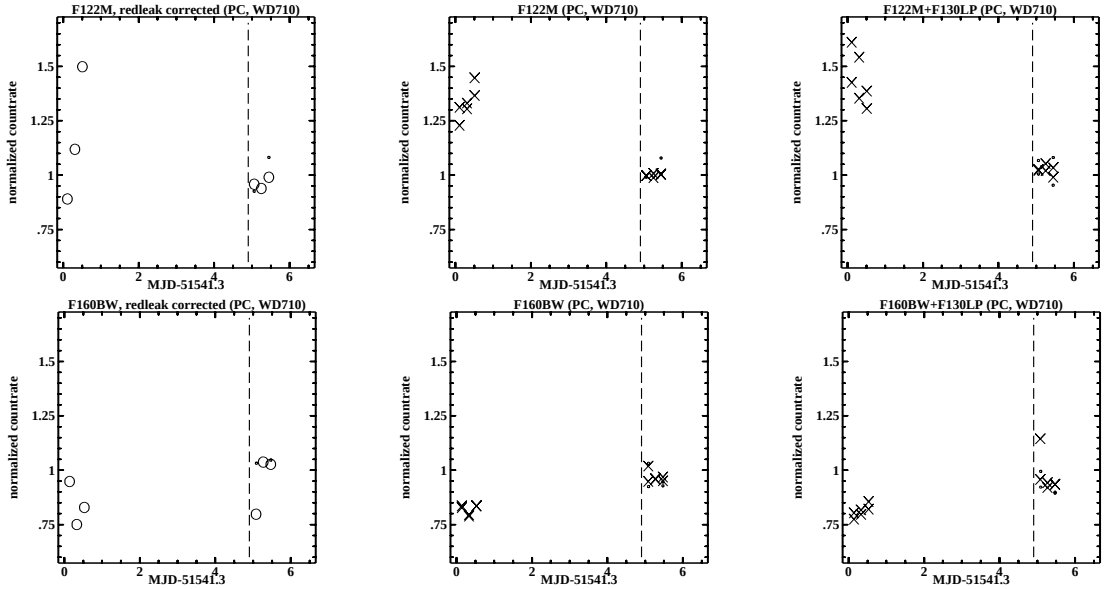

In F122M, the redleak-corrected values for WD 0710+741 (top left plot in Figure 4.1) show a large amount of scatter at -57 C (~+/- 30%) while the values at -88 C are better behaved (~+/-5%). A large scatter at -57 C was not entirely unexpected, due to the faintness of the target and the high level of dark current at the warmer temperature. The absolute F122M photometry level at -88 C is within 5% of the baseline measurements. In F160BW at -57 C, the redleak-corrected data show less scatter (<+/-10%) than in F122M and at -88 C, excluding the one outlier, the measurement scatter is only ~+/-5%, with the absolute level within 5% of the baseline value.

The scatter in the GRW+70D5824 data at -57 C is much smaller than for the fainter WD701+741, only ~+/-5%. However, the absolute level of the redleak-corrected values at -88 C are below the pre-SMOV3a values. When normalized to the November 1996 baseline data, the data are ~5-10% low in F122M and ~20% low in F160BW. The data were also normalized to a baseline set taken closer in time to SMOV3a, though only the F160BW data were available; these data are shown as squares in Figure 4.2. In this case, the -88 C data fall only ~5% below the pre-SMOV3a data.

Figure 4.2: SMOV3a Lyman-α throughput check results for GRW+70D5824. Top row of plots are for F122M, bottom row plots are for F160BW. Plots from left to right are the normalized count rates for: redleak-corrected, single filter, and crossed filter data, as a function of Modified Julian date. Dashed line marks the date of the cooldown from -57 C to -88 C. For both far-UV filters, count rates normalized to Nov. 1996 measurements are denoted with crosses (single and crossed filter images) and circles (redleak-corrected averages of each image pair). Count rates for F160BW were also normalized to Aug. 1997 (squares).

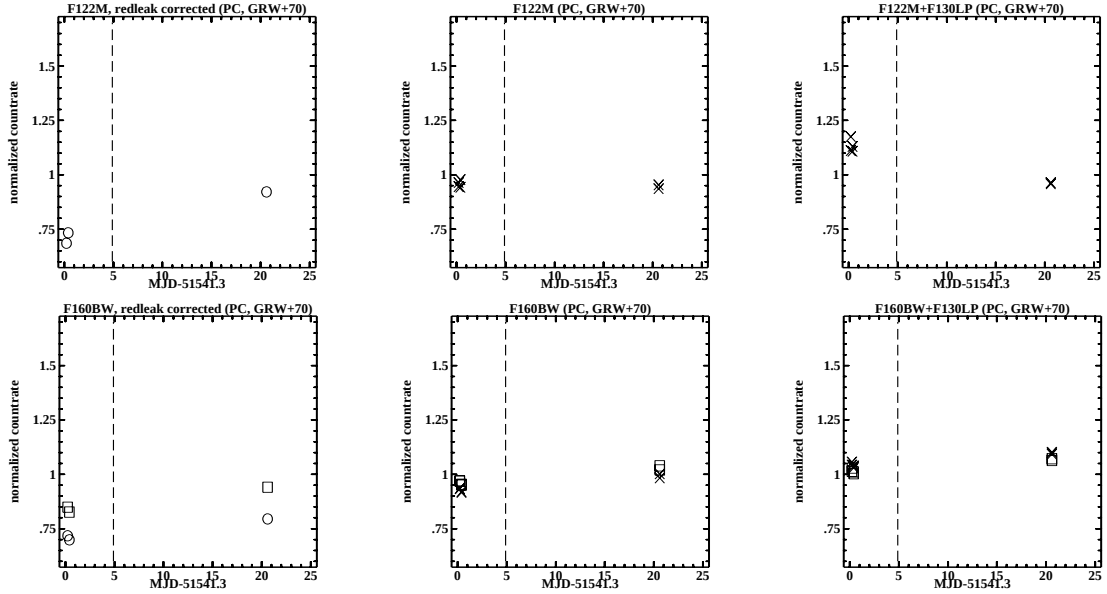

For GRW+70D5824, the formal errors are ~1-3% for the individual measurements and 3-4% for the redleak-corrected results; for WD 0710+741, those errors are ~5-7% and 8-9%, respectively. However, we estimate the errors are closer to 10-20% due to the following factors.

- WD 0710+741 is relatively faint, with count rates a factor of 10 lower than those for GRW+70D5824; at the same time, scheduling restrictions prohibited increasing exposure times to match the GRW+70D5824 counts. Total counts for the two stars were typically ~4500 DN vs. 870 DN (F122M) and 3160 DN vs. 1350 DN (F160BW). It was extremely difficult to identify WD 0710+741 in the -57 C datasets, even after recalibrating using a post-SM3a dark generated from five dark frames taken at -57 C.
- No contamination rate estimates exist for F122M; the rate for F160BW (~0.6%/day) was used for both F122M and F160BW. This could be particularly significant for the baseline WD 0710+741 measurements since they required a large correction (26 days).
- The flatfields for F122M and F160BW are based on ground thermal vacuum test data; no on-orbit updates have been made. The F160BW flatfield is known to be somewhat noisy (see, e.g., STAN 33, Aug. 1998): the RMS noise near the center of the PC is nearly ~20% and there are a few individual pixel errors nearly a factor of 6 larger. Note, however, that any individual pixel outliers, at least, would have been removed in the manual cosmic ray / hot pixel cleanup.
- There are no flatfields for the crossed filter combinations; as noted in the data section, the uncrossed flatfields were used for all images.

- The redleak for these stars is appreciable (more than 60% in F122M and ~70% in F160BW). Any errors in either the single or crossed filter data propagate into the redleak-corrected results. In addition, the redleak correction was a very simple one: subtraction of the crossed filter results from the single filter results. No correction was made to account for less than perfect throughput in F130LP (~0.95 beyond 4000A).
- There is a considerable amount of scatter in the normal F160BW routine monitoring observations of GRW+70D5824 (images crossed with F130LP are not routinely taken). For example, since 1996, the contamination-corrected PC F160BW observations taken less than 5 days after a decon have fluctuated by about 8% (based on data from Gonzaga et al., WWW memo).
- In addition, a small long-term increase in post-decon measurements of GRW+70D5824 has been observed in F160BW in PC (Baggett & Gonzaga, 1998). The effect is ~5% between late 1996 and early 2000. Note that this particular effect would, of course, move the redleak-corrected values lower (Figure 4.2, lower left plot).

For these reasons, the results for SMOV3a are considered to be within the measurement error and we conclude that the Lyman-α throughput measurements for SMOV3a in PC did not show any significant changes compared to pre-SM3a. The WFPC2 pick-off mirror appears to have been protected from any significant contamination.

Acknowledgements

We thank S. Casertano for selecting the alternate standard star and coordinating the SMOV3a-related activities, S. Gonzaga for writing the Lyman-α SMOV proposals, and S. Gonzaga for comments on this report.

References

Baggett, S., and Gonzaga, S., 1998, “WFPC2 Long-Term Photometric Stability,” WFPC2 ISR 98-03.

Biretta, J., Heyer, I., Baggett, S., Casertano, S., Fruchter, A., Gonzaga, S., Krist, J., Lallo, M., McMaster, M., Mutchler, M., O’Dea, C., Stiavelli, M., Suchkov, A., and Whitmore, B., 1997, “Results of the WFPC2 Post-Servicing Mission-2 Calibration Program,” ISR 97-09.

Casertano, S., Gonzaga, S., Biretta, J., and Balleza, J., 1999, “Summary of WFPC2 SM3a Plans”, ISR 99-03.

Gonzaga, S., Ritchie, E., Baggett, S., Casertano, S., Whitmore, B., and Mutchler, M., Standard Star Monitoring Data, memo routinely updated on WWW. Accessible via the WFPC2 Documentation page under Calibration Monitoring or directly at http://www.stsci.edu/instruments/wfpc2/Wfpc2_memos/wfpc2_stdstar_phot3.html

MacKenty, J., and Baggett, S., 1996, “WFPC2 Throughput Stability in the Extreme Ultraviolet,” WFPC2 ISR 96-07.

McCook, G. P., and Sion, E. M., 1987, ApJS **65**, 603.

O’Dea, C., Baggett, S., and Gonzaga, S., 1997, “Results of the WFPC2 SM-2 Lyman-α Throughput Check,” TIR 97-05.

Stiavelli, M., Biretta, J., Baggett, S., Gonzaga, S., Mutchler, M., 1997, “SM-2 UV Monitoring and Cool-down Procedure (PIE 7016 and 7122),” WFPC2 TIR 97-02.

Turnshek, D. A., Bohlin, R. L., Williamson, R. L., Lupie, O. L., and Koornneef, J., 1990, AJ **99**, 1243.

5: Photometric throughput

by Al B. Schultz, S. Gonzaga, and S. Casertano

Note: these results have been reported independently in WFPC2 Technical Instrument Report (TIR) 00-03, *SM3a SMOV WFPC2 Photometry Check*, by Al B. Schultz, Shireen Gonzaga, and Stefano Casertano.

Summary: A check of the photometric throughput of the WFPC2 was performed on January 18, 2000 (program ID: 8496). The standard star GRW+70d5824 was observed with a selection of filters and the standard star was centered in each of the four CCDs. The observations were obtained ~0.6 day after the WFPC2 DECON on January 17, 2000 (program ID: 8491, visit 55). The data indicate that any changes in the photometric throughputs due to SM3a are less than 1% in most of the visible wavelength filters, and less than a few percent in the UV filters. The measured UV throughputs are consistent with the long term trends of the UV sensitivity. The response of the WFPC2 has essentially not changed.

Photometry Monitor Observations

Observations of standard star GRW+70d5824 (V = 12.7, B-V = -0.09) for the photometry check were obtained on January 18, 2000 (program ID: 8496) which was approximately 0.6 day following the DECON on January 17, 2000. The star was positioned in the center of a camera during four 1-orbit visits, one visit per camera. The respective single camera images were read out and sent to the ground for analysis. Observations were obtained with filters F160BW, F170W, F185W, F218W, F255W, F300W, F336W, F439W, F555W, F675W, and F814W. Inspection of the data showed that the central pixel of the star image was saturated in two observations, u60g010ar and u60g0206r. Table 5.1 lists the observations.

Table 5.1:8496 photometry monitor observations (* - central pixel of stellar image was saturated).

filter	PC1	PC1 exptime (sec.)	WF2	WF3	WF4	WF exptime (sec.)
F160BW	u60g0101r	200.0	u60g0201r	u60g0301r	u60g0401r	100.0
F170W	u60g0102r	40.0	u60g0202r	u60g0302r	u60g0402r	40.0
F185W	u60g0103r	100.0	u60g0203r	u60g0303r	u60g0403r	100.0
F218W	u60g0104r	40.0	u60g0204r	u60g0304r	u60g0404r	40.0
F255W	u60g0105r	80.0	u60g0205r	u60g0305r	u60g0405r	40.0
F300W	u60g0106r	12.0	u60g0206r*	u60g0306r	u60g0406r	12.0
F336W	u60g0107r	14.0	u60g0207r	u60g0307r	u60g0407r	12.0
F439W	u60g0108r	14.0	u60g0208r	u60g0308r	u60g0408r	8.0
F555W	u60g0109r	3.5	u60g0209r	u60g0309r	u60g0409r	2.3
F675W	u60g010ar*	8.0	u60g020ar	u60g030ar	u60g040ar	4.0
F814W	u60g010br	14.0	u60g020br	u60g030br	u60g040br	7.0

Calibration & Reducing the Data

The OPUS pipeline calibrated data were used for the analysis. No other calibration steps were performed. The IRAF task **imedit** was used to remove cosmic rays around the stars from the individual CCD frames.

Photometry was performed using the **apphot** task **phot** with the star positions manually identified for each camera as input. For the PC1 frames, a photometry aperture radius of 11 pixels was used with the sky fitting region parameters set to annulus=32 pixels and dannulus=11 pixels. For the WF frames, a photometry aperture radius of 5 pixels was used with the sky fitting region parameters set to annulus=15 pixels and dannulus=5 pixels. The sky fitting algorithm was set to “ofilter.” The centering algorithm was set to “centroid” with parameters cbox=5 and maxshif=1. The photometry values are listed in Table 5.2. For Table 5.2, the table headers are:

filter - WFPC2 filter used.

mjd - modified Julian Date (Julian Date - 2400000.5) for the observation.

flux - the total corrected counts in the respective aperture.

ct_rate - actual count rate (DN/s) for the respective aperture.

ctr_err - measurement uncertainty of the count rate.

Table 5.2: 8496 PC1 photometry. Pre-SMOV zero points were used to determine the respective HST filter magnitudes (mag). The F675W filter observation was saturated.

filter	mjd	flux	ct_rate	ctr_err	mag
F160BW	51561.5564	16736.0	83.680	0.1808	9.055
F170W	51561.5613	6685.349	167.133	0.6054	9.620
F185W	51561.5634	9916.14	99.161	0.2867	9.878
F218W	51561.5661	5407.032	135.175	0.5562	10.252
F255W	51561.5682	12376.73	154,709	0.3944	10.784
F300W	51561.5710	11508.17	959.014	2.5439	11.230
F336W	51561.5731	10667.61	761.972	2.1084	11.577
F439W	51561.5752	12334.69	881.049	2.2628	12.119
F555W	51561.5773	13121.24	3748.925	9.2872	12.865
F675W	-	-	-	-	-
F814W	51561.5814	18823.04	1344.502	2.7356	14.335

Table 5.3: 8496 WF2 photometry. Pre-SMOV zero points were used to determine the respective HST filter magnitudes (mag). The F300W filter observation was saturated.

filter	mjd	flux	ct_rate	ctr_err	mag
F160BW	51561.6231	7788.212	77.8821	0.23909	9.269
F170W	51561.6259	7684.733	192.1183	0.5975	9.573
F185W	51561.6279	10283.53	102.8353	0.2754	9.934
F218W	51561.6307	5605.957	140.148	0.5132	10.292
F255W	51561.6328	6561.638	164.0409	0.5559	10.775
F300W	-	-	-	-	-
F336W	51561.6370	9221.045	768.4204	2.1719	11.592
F439W	51561.6391	7196.472	899.5590	2.8948	12.107
F555W	51561.6411	8712.167	3787.8986	11.0653	12.872
F675W	51561.6432	8516.099	2129.0247	6.3048	13.709
F814W	51561.6453	9847.85	1406.8357	3.8597	14.299

An IRAF script was used to extract selected fields from the **phot** task output files. The script also determines the count rate (ct_rate) and the associated uncertainty of the count rate (ctr_err). The equations used to determine the count rate error are presented below:

sigskysqd = stdev*stdev

errorsq = ((abs(sum - msky*area))/gain) + sigskysqd*(area + (area*area/nsky))

ctr_err = sqrt(errorsq)/itime

Table 5.4: 8496 WF3 photometry. Pre-SMOV zero points were used to determine the respective HST filter magnitudes (mag).

filter	mjd	flux	ct_rate	ctr_err	mag
F160BW	51561.6904	6619.847	66.1984	0.2228	9.257
F170W	51561.6932	6247.583	156.1895	0.5419	9.665
F185W	51561.6953	8538.938	85.3893	0.2523	10.019
F218W	51561.6981	5152.403	128.8100	0.4966	10.296
F255W	51561.7002	6427.683	160.6920	0.5515	10.751
F300W	51561.7023	12038.32	1003.1933	2.4847	11.198
F336W	51561.7043	9411.546	784.2955	2.2065	11.567
F439W	51561.7064	6963.971	870.4963	2.8739	12.154
F555W	51561.7085	8578.42	3729.7478	11.0090	12.874
F675W	51561.7106	8233.615	2058.4037	6.1868	13.705
F814W	51561.7127	9257.141	1322.4487	3.7502	14.368

Table 5.5: 8496 WF4 photometry. Pre-SMOV zero points were used to determine the respective HST filter magnitudes (mag).

filter	mjd	flux	ct_rate	ctr_err	mag
F160BW	51561.8245	7037.982	70.3798	0.2294	9.277
F170W	51561.8273	6842.04	171.0510	0.5713	9.627
F185W	51561.8293	9868.771	98.6877	0.2714	9.915
F218W	51561.8321	5519.535	137.9883	0.5152	10.260
F255W	51561.8342	6623.003	165.5750	0.5600	10.739
F300W	51561.8363	11957.92	996.4933	2.4812	11.213
F336W	51561.8384	9391.141	782.5950	2.2068	11.570
F439W	51561.8404	7119.119	889.8898	2.9009	12.124
F555W	51561.8425	8729.536	3795.4504	11.1173	12.862
F675W	51561.8446	8431.069	2107.7672	6.2936	13.699
F814W	51561.8467	9771.252	1395.8931	3.8522	14.316

where the parameters (output **phot** fields) are defined as follows:

sum = total number of counts including sky in aperture

area = area of the aperture in square pixels

itime = exposure time (exptime) header keyword value

msky = sky value per pixel stdev = standard deviation of sky value

gain = gain image header keyword value

nsky = number of sky pixels

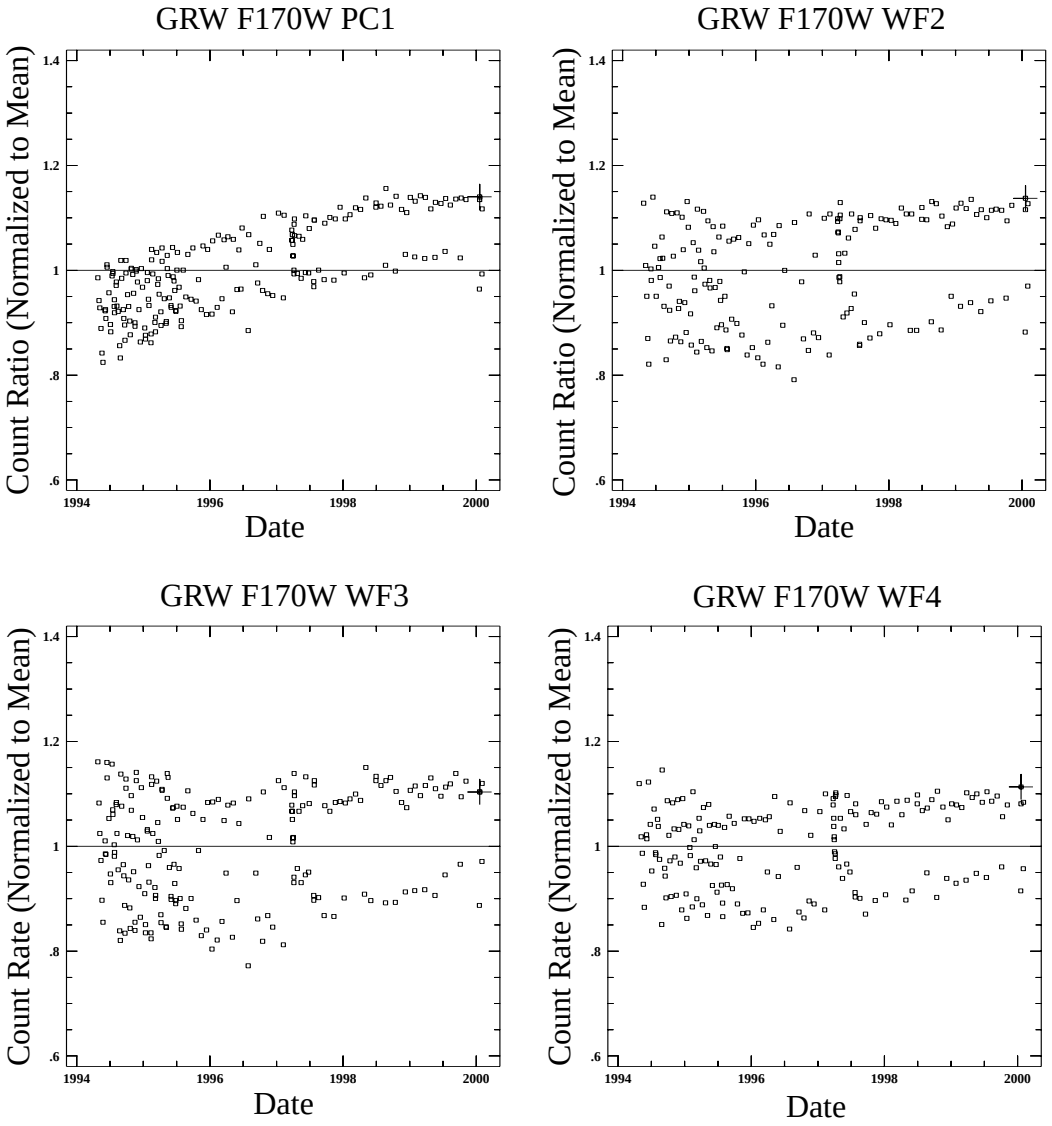

Figure 5.1: Photometric monitoring of standard star GRW+70D5824. The observations span a time interval from May 1, 1994 to January 31, 2000. The observations executed twice for each decontamination cycle, a pre-DECON and a post-DECON visit. The 8496 data points are marked with a “cross-hair”. The UV sensitivity has been recovered.

UV Sensitivity

The UV sensitivity of the WFPC2 will change depending upon the amount of contamination and will vary between DECONs. Normally the monitor program is executed before and after the decontamination procedures to monitor any change to the UV throughput.

The 8496 calibration program executed approximately 0.6-1.2 days following the DECON on January 17, 2000.

Figure 5.1 presents the UV filter F170W results compared with observations obtained prior to the HST entering Safe mode on November 13, 1999. The measurements have been normalized to the mean count rate. The 8496 measurements are marked with a “cross-hair.” The figure indicates that the UV sensitivity has been recovered, and it also shows the long term trend of increased count rates for the UV throughput (Baggett and Gonzaga 1998).

Photometric Response

Calibration data for filters F185W and F300W were retrieved from the Archive. Filter F185W has not been used for the monitor program, and filter F300W was dropped from the monitor program. The data for these two filters were recalibrated using the on-the-fly calibration (OTFC) option within StarView. The data were reduced in an identical manner to the 8496 data.

Table 5.6:WFPC2 F185W filter photometry, pre-SMOV data.

camera	date	mjd	flux	ct_rate	ctr_err	dsd
PC1	25-Aug-97	50685.3390	3872.957	96.823	0.4876	5.24
	7-Sep-97	50698.2182	3557.605	88.940	0.4671	18.12
	13-Oct-98	51099.1252	3542.301	88.557	0.4732	28.02
	17-Oct-98	51103.2884	3689.915	92.247	0.4780	3.17
WF2	25-Aug-97	50685.3981	3935.136	98.378	0.4364	5.30
	7-Sep-97	50698.2738	3516.207	87.905	0.4112	18.18
WF3	25-Aug-97	50685.5050	3281.393	82.034	0.4022	5.41
	7-Sep-97	50698.3474	2833.934	70.848	0.3751	18.25
	13-Oct-98	51099.1856	2739.333	68.483	0.3688	28.08
	17-Oct-98	51103.3495	3536.039	88.400	0.4131	3.24
WF4	25-Aug-97	50685.5779	3748.342	93.708	0.4310	5.48
	7-Sep-97	50698.4085	3408.931	85.223	0.4162	18.31

Table 5.7:WFPC2 F300W filter photometry, pre-SMOV data.

camera	date	mjd	flux	ct_rate	ctr_err	dsd
PC1	29-Jan-99	51207.8571	11760.22	980.0183	2.570046	1.81
	09-Sep-99	51430.7133	11517.96	959.8300	2.53666	0.65
WF2	13-Oct-98	51099.2134	9271.048	927.1048	2.613457	28.11

camera	date	mjd	flux	ct_rate	ctr_err	dsd
	17-Oct-98	51103.3772	9772.944	977.2944	2.687061	3.26
WF3	13-Oct-98	51099.1897	9323.223	932.3223	2.625705	28.09
	17-Oct-98	51103.3536	9878.305	987.8305	2.702031	3.24
WF4	13-Oct-98	51099.2078	9567.56	956.7560	2.678465	28.11
	17-Oct-98	51103.3717	10080.78	1008.0780	2.742469	3.262

Tables 5:8-11 presents the 8496 photometric measurements compared to the pre-Safing measurements closest in time to the 8496 observations. The photometric monitor pre-Safing event measurements can be found on the STScI WFPC2 web page (Gonzaga et al. 2000). The 8496 measurements have been ratioed with the pre-Safing event measurements.

Table 5.8:PC1 photometry, pre-SMOV and 8496 count rates (dsd: days since DECON). The 8496 F675W filter observation was saturated.

filter	Date	dsd	ct_rate	Date	dsd	ct_rate	ratio
F160BW	09-Jun-99	0.6	84.5668	18-Jan-00	0.87	83.680	0.989
F170W	04-Nov-99	1.3	166.4179	18-Jan-00	0.87	167.133	1.004
F185W	17-Oct-98	3.1	92.247	18-Jan-00	0.87	99.161	1.074
F218W	09-Sep-99	0.7	134.7721	18-Jan-00	0.88	135.161	1.002
F255W	20-May-99	1.6	157.7611	18-Jan-00	0.88	154.709	0.980
F300W	09-Sep-99	0.6	959.8300	18-Jan-00	0.88	959.014	0.999
F336W	09-Sep-99	0.7	755.7880	18-Jan-00	0.88	761.972	1.008
F439W	09-Sep-99	0.7	879.8325	18-Jan-00	0.89	881.049	1.001
F555W	04-Nov-99	1.3	3715.3520	18-Jan-00	0.89	3748.925	1.009
F675W	09-Sep-99	0.7	2073.9580	18-Jan-00	0.89	-	-
F814W	09-Sep-99	0.6	1329.2300	18-Jan-00	0.89	1344.502	1.011

Table 5.9:WF2 photometry, pre-SMOV and 8496 count rates (dsd: days since DECON). The 8496 F300W filter observation was saturated.

filter	Date	dsd	ct_rate	Date	dsd	ct_rate	ratio
F160BW	09-Oct-99	3.5	77.1258	18-Jan-00	0.93	77.882	1.009
F170W	04-Nov-99	1.3	189.8454	18-Jan-00	0.94	192.118	1.011
F185W	25-Aug-97	5.3	98.378	18-Jan-00	0.94	102.835	1.045
F218W	20-Jun-99	3.9	142.5608	18-Jan-00	0.94	140.148	0.983
F255W	09-Oct-99	3.5	165.0441	18-Jan-00	0.94	164.040	0.993
F300W	17-Oct-98	3.26	977.2944	18-Jan-00	0.94	-	-
F336W	09-Oct-99	3.5	776.2471	18-Jan-00	0.95	768.420	0.989
F439W	09-Oct-99	3.5	901.1561	18-Jan-00	0.95	899.559	0.998
F555W	09-Oct-99	3.5	3767.0380	18-Jan-00	0.95	3787.898	1.005
F675W	20-Jun-99	3.9	2143.8780	18-Jan-00	0.96	2129.024	0.993
F814W	09-Oct-99	3.5	1374.0420	18-Jan-00	0.96	1406.935	1.023

Table 5.10:WF3 photometry, pre-SMOV and 8496 count rates (dsd: days since DECON).

filter	Date	dsd	ct_rate	Date	dsd	ct_rate	ratio
F160BW	04-Nov-99	1.3	68.4227	18-Jan-00	1.00	66.198	0.967
F170W	04-Nov-99	1.3	159.0743	18-Jan-00	1.01	156.189	0.981
F185W	17-Oct-98	3.2	88.400	18-Jan-00	1.01	85.389	0.965
F218W	04-Nov-99	1.3	130.4968	18-Jan-00	1.01	128.810	0.987
F255W	04-Nov-99	1.3	168.5777	18-Jan-00	1.01	160.692	0.953
F300W	17-Oct-98	3.2	987.8305	18-Jan-00	1.01	1003.198	1.015
F336W	04-Nov-99	1.3	770.5485	18-Jan-00	1.02	784.295	1.017
F439W	04-Nov-99	1.3	875.7900	18-Jan-00	1.02	870.496	0.993
F555W	04-Nov-99	1.3	3722.2030	18-Jan-00	1.02	3729.747	1.002
F675W	26-Mar-99	1.0	2056.8380	18-Jan-00	1.02	2058.403	1.000
F814W	04-Nov-99	1.3	1329.2300	18-Jan-00	1.02	1322.448	0.994

Table 5.11:WF4 photometry, pre-SMOV and 8496 count rates (dsd: days since DECON).

filter	Date	dsd	ct_rate	Date	dsd	ct_rate	ratio
F160BW	10-Aug-99	0.8	70.4693	18-Jan-00	1.14	70.379	0.998
F170W	04-Nov-99	1.3	165.8059	18-Jan-00	1.14	171.051	1.031
F185W	25-Aug-97	5.4	93.708	18-Jan-00	1.14	98.687	1.053
F218W	10-Aug-99	0.8	139.7012	18-Jan-00	1.14	137.988	0.987

filter	Date	dsd	ct_rate	Date	dsd	ct_rate	ratio
F255W	10-Aug-99	0.8	166.4179	18-Jan-00	1.15	165.570	0.994
F300W	17-Oct-98	3.26	1008.078	18-Jan-00	1.15	996.403	0.988
F336W	10-Aug-99	0.8	789.2235	18-Jan-00	1.15	782.950	0.992
F439W	10-Aug-99	0.8	889.6107	18-Jan-00	1.15	889.889	1.000
F555W	10-Aug-99	0.8	3746.2780	18-Jan-00	1.15	3795.450	1.013
F675W	10-Aug-99	0.8	2110.5710	18-Jan-00	1.16	2107.767	0.998
F814W	11-Aug-99	0.8	1370.2510	18-Jan-00	1.16	1395.893	1.018

Figure 5.2 presents in graphical form the ratio (8496/pre-Safing measurements) versus wavelength for each camera. The trends indicate a normal recovery of sensitivity with a slight increase in sensitivity, ~1-2%. The data spike at wavelength 1907 Å is from the F185W filter data. The elevated level of the ratio for this filter, except for WF3, is due to the increasing trend over time of the far-UV throughput (as seen in Figure 5.1) and the comparison data for this filter are earlier than for other pre-SM3a filter data.

The WF3 UV filter sensitivity ratios (as seen in Figure 5.2) are different than for the other cameras, indicating a slight decrease in sensitivity. The decreases in the WF3 UV sensitivity are -3.2% for F160BW, -1.8% for F170W, -3.4% for F185W, -1.3% for F218W, and -4.6% for F255W. This does not result from positioning of the target on the WF3 CCD as the visible filters show a slight improvement of the count rate. See “Appendix I - WF3 Calibration” on page 29 for a discussion about the positions of the calibration target on the WF3 CCD.

The positions of the calibration target on the CCDs for the January 18, 2000 data (post-SM3a) are consistently closer to the apex of the pyramid and the readout amplifier than for the pre-SM3a data. Due to less loss of charge resulting from CTE, the count rates for the visible filter data should be slightly higher than for the pre-SM3a count rates.

Conclusions and Recommendations

The WFPC2 calibration program 8496 executed post-DECON. Observations of the standard star GRW+70D582 were obtained with each camera and with the normal selection of monitor filters (11 filters). Two images were saturated, u60g010ar (PC1) and u60g0206r (WF2). The measurements indicate that the SM3a DECONs prior to January 18, 2000 removed most if not all of the contamination and the UV sensitivity continues to show an increase with time. Each camera performed as expected.

The data indicate that the throughputs for the optical filters, except for the F814W filter, are consistent with no change exceeding ~1% with the throughput for F814W filter consistent with no change exceeding ~2%. Except for the F185W filter, the UV throughput increased by ~1% when compared to pre-SM3a measurements. The WF3 UV

throughputs are different than for the other cameras, exhibiting an as yet unexplained slight decrease of ~1-2%, but they are consistent with the long term trends of WF3 (as can be seen in Figure 5.1). The throughputs show that the WFPC2 suffered no ill effects from the Safing event on November 13, 1999.

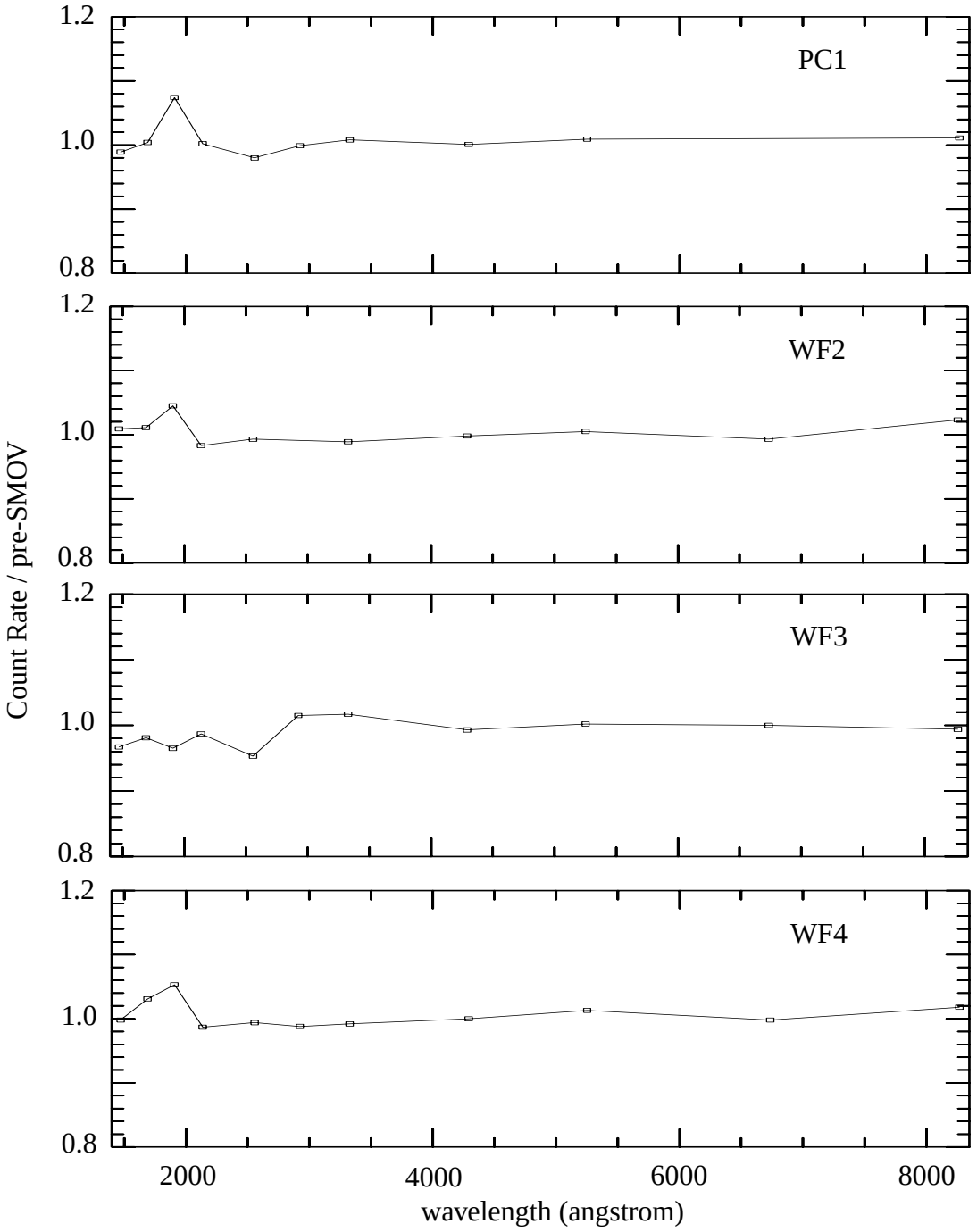

Figure 5.2: Ratio of 8496 / pre-SMOV 2000 measurements. The data spike at wavelength 1907 Å is due to the F185W filter data. The WF3 UV sensitivity ratio is different than for the other cameras.

References

Baggett, S. and Gonzaga, S. 1998, WFPC2 Long-Term Photometric Stability, WFPC2-ISR-98-03.

Gonzaga, S., Ritchie, C., Baggett, S., Casertano, S., Whitmore, B., and Mutchler, M. 2000, “Standard Star Monitoring Memo”, available at URL
http://www.stsci.edu/instruments/wfpc2/Wfpc2_memos/wfpc2_stdstar_phot3.html

Appendix I - WF3 Calibration

The WF3 UV sensitivity ratio (see Figure 5.2) is different than for the other cameras. This could be due to differences in positioning of the calibration target GRW+70d5824 on the WF3 CCD between observations. Table 12 presents the positions of the target on the WF3 CCD. The positioning of the target on January 18, 2000, post-SM3a data, is consistently closer to the apex of the pyramid and the readout amplifier than for the pre-SM3a data. Due to less loss of charge resulting from CTE, the post-SM3a count rates should be higher than the pre-SM3a count rates. In addition, the target position on November 4, 1999 for the F170W filter observation is extremely close to the pyramid apex compared to other observations. The additional charge for the F170W filter count rate would explain the lack of improvement in the ratio for this filter, but positioning on the CCD of the target in general does not explain the UV sensitivity ratio for WF3.

Table 5.12:WF3 photometry, pre- and post-SMOV observations.

filter	Date	Obs.	x,y (pixels)	Date	Obs.	x,y (pixels)
F160BW	04-Nov-99	u5if7801r	431.97,433.04	18-Jan-00	u60g0301r	419.50,426.31
F170W	04-Nov-99	u5if780br	230.30,230.81	18-Jan-00	u60g0302r	419.60,426.34
F185W	17-Oct-98	u4s6040dr	439.02,435.21	18-Jan-00	u60g0303r	419.75,426.39
F218W	04-Nov-99	u5if7802r	432.20,433.11	18-Jan-00	u60g0304r	419.79,426.39
F255W	04-Nov-99	u5if7803r	432.51,432.48	18-Jan-00	u60g0305r	420.06,425.74
F300W	17-Oct-98	u4s6040lr	432.42,419.02	18-Jan-00	u60g0306r	419.75,426.03
F336W	04-Nov-99	u5if7804r	432.21,433.01	18-Jan-00	u60g0307r	419.77,426.29
F439W	04-Nov-99	u5if7805r	432.19,432.85	18-Jan-00	u60g0308r	419.79,426.03
F555W	04-Nov-99	u5if7806r	432.03,432.79	18-Jan-00	u60g0309r	419.62,426.00
F675W	26-Mar-99	u42w460dr	430.05,422.28	18-Jan-00	u60g030ar	419.88,425.51
F814W	04-Nov-99	u5if7807r	432.00,432.68	18-Jan-00	u60g030br	419.50,425.90

6: Point spread function

by Adam Riess and Shireen Gonzaga

Summary: The Point-Spread Function (PSF) of WFPC2 has been verified through observations of an isolated bright star and of a rich star field. No significant variations in the PSF have been found.

Figure 6.1: Radial profile of stellar counts on the WFPC2 PC for stars in ω Cen observed after SM3a. The stars have been normalized by the total counts in a 5 PC pixel aperture. The resulting composite curve from stars near the center of the chip is compared to the fiducial Gaussian model of FWHM=0.”064.

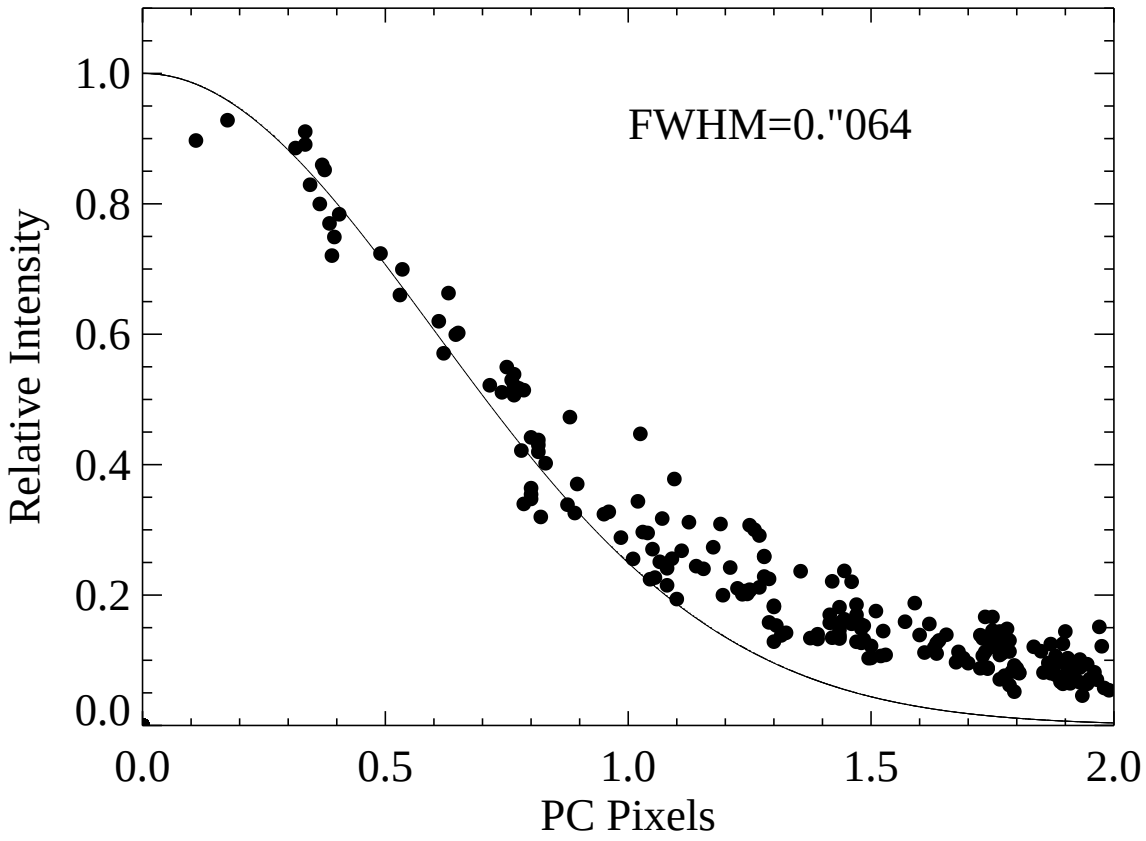

Observation and Analyses

Following the methodology of Biretta et al. (1997) employed after SM2, images of ω Cen were obtained to characterize the PSF of the WFPC2 after SM3a. Four dithered positions of ω Cen were obtained through the F555W filter on January 10, 2000, each for 100 seconds. The dithers were substepped by one-third of a pixel in each coordinate, in order to improve the sampling of the PSF. The images were then combined using the **dither**

routines found in the IRAF package **stsdas.analysis.dither**. We followed the procedures as described in The Drizzling Cookbook (Gonzaga et al. 1998). Our final drizzles images employed a scale of half the original pixel size and a pixel footprint of 0.8.

The pixel scale in the PC is more than a factor 2 smaller than in the WF cameras. For this reason, the observed PC PSF is a better indicator of the telescope and instrumental optics than the observed WF PSF which is heavily dominated by the pixel response function (i.e., charge diffusion). For this reason we have characterized the PSF using PC data.

We chose a number of bright stars which were not saturated, well isolated, and located near the center of the PC. For each of these stars, we scaled the intensity by the counts contained in a 5 PC pixel aperture and plotted this result as a function of the pixel distance from the center (determined from a 5 PC pixel box). The composite data from the stars is show in Figure 6.1. This data is compared to a Gaussian curve with a FWHM=0.064", the best-model employed for this same exercise by Biretta et al. (1997) after SM2. The shape of the PSF appears unchanged with respect to the previous results; as in 1997, the PSF is well-described by the Gaussian curve within the half-maximum point, and shows an excess of up to 10% of the peak with respect to the Gaussian outside that radius. The . Beyond this range the stellar counts have intensities relative to peak which are ~10% greater than the curve. Both FWHM and overall shape of the PSF are therefore unaffected by the Servicing Mission 3a.

7: Camera internals

by Chris O'Dea, Inge Heyer, Sylvia Baggett

Summary: We report on the stability of WFPC2 with special attention to any potential changes due to SM3a as determined from internal calibration observations, including read noise, dark current, internal flats, gain ratios, and position of the K-spots. We find no significant changes in the read noise at either gain 7 or 15. Dark current increases by a few percent (2 to 8% depending on chip), consistent with the steady increase found by Baggett et al (1999). Small changes (0.1% to 1%) in the pattern and relative intensity of the INTFLAT and VISFLAT images are compatible with differential variations in the light output of the lamps. The K-spots shifted on average by about 10 milliarcseconds between November 1999 and January 2000, also consistent with the known time evolution of the K-spot positions. Overall, the WFPC2 appears to be very stable, exhibiting only the minor changes expected due to known low level variability.

Note: An extended version of this report has been released independently as WFPC2 Technical Instrument Report (TIR) 00-04, Camera Internals, by Chris O'Dea, Inge Heyer and Sylvia Baggett.

Introduction

We describe the results of the internal WFPC2 calibration observations (programs 8491 and 8498). These were obtained as part of Servicing Mission Observatory Verification (SMOV) following the third HST servicing mission (SM3a) in January, 2000. The goal of these observations was to ensure that there was no significant change in the basic WFPC2 instrument health and internal calibrations. The structure of this report generally follows that for SM2 by Mutchler and Stiavelli (1997, hereafter MS97).

Observations in 8498 were done during the 1st and 3rd week after Bright Earth Avoidance (BEA). Internal observations on the 2nd and 4th weeks were part of the DECON proposal (8491). Bias observations are obtained at both gain settings. INTFLATs were obtained in the five photometric filters at gain 7 and in F555W for gain 15. A pair of K-spots were taken at gain 15. Five 30 min darks were obtained along with one dark with CLOCKS=YES. A sweep of the VISFLATs was obtained in gain 7 in the five photometric filters and in both gains in FR533N.

Analysis

Table 7.1:WFPC2 Read Noise.

chip	gain	Pre-SM3a[a] (DN)	Pre-SM3a (e^-)	Post-SM3a (DN)	Post-SM3a (e^-)	change (e^-)
PC1	7	0.761 (0.001)	5.418 (0.007)	0.770 (0.003)	5.482 (0.021)	0.064 (0.028)
WF2	7	0.735 (0.003)	5.233 (0.021)	0.736 (0.002)	5.233 (0.014)	0.00 (0.035)
WF3	7	0.737 (0.002)	5.085 (0.014)	0.755 (0.007)	5.209 (0.049)	0.124 (0.063)
WF4	7	0.740 (0.010)	5.254 (0.071)	0.755 (0.007)	5.240 (0.014)	-0.014 (0.085)
PC1	15	0.519 (0.014)	7.261 (0.196)	0.755 (0.007)	7.764 (0.042)	0.503 (0.238)
WF2	15	0.519 (0.014)	7.525 (0.203)	0.545 (0.009)	7.903 (0.131)	0.378 (0.334)
WF3	15	0.566 (0.003)	7.896 (0.042)	0.552 (0.010)	7.700 (0.140)	-0.196 (0.182)
WF4	15	0.607 (0.015)	8.467 (0.209)	0.565 (0.028)	7.882 (0.390)	-0.585 (0.599)

a. Pre-SM3a corresponds to Oct-Nov 1999, and Post-SM3a corresponds to Jan 2000. Numbers in the table have been corrected for the factor of square root of 2. The counts in DN have been converted to electrons using the values for the gain in Table 4.3 of the WFPC2 Handbook. The uncertainties are the standard deviation of the mean value and do not include the propagation of error from the gains in the conversion to electrons.

Biases

The goal was to measure any changes in the biases to a precision of about 1.4 electrons/pixel (0.2 DN and 0.1 DN for gain 7 and 15 respectively). We obtained a total of eight biases in each gain setting post-SMOV. We retrieved the same number of pre-SM3a biases taken with program 8444 from the Oct.-Nov. 1999 period (starting just before the safing and working backwards). There were some small bias jumps in the data but no other

anomalies. For each group of biases, we picked a “clean” example and subtracted it from the other seven in the group. This removes any constant structure in the biases. We determined the standard deviation of the subtracted bias frames which is equal to the read noise times square root of 2. The results are given in Table 7.1.

Given the statistical uncertainties, there are no significant changes in the read noise.

We combined the biases with cosmic ray rejection to make a “master” image for each gain pre- and post-SM3a. The post-SM3a master bias was subtracted from the pre-SM3a master bias and we examined the difference image for changes to the bias structure. There were no obvious changes, either in the images themselves or in the row and column averages. There is a low-level “rumble” in the averages, at the level of 0.01-0.02 DN rms. These changes are probably not related to SM3a, since similar variations have been seen at other times, and have a negligible effect on the science data.

Table 7.2: Dark Current Pre-SM3a, gain 7.

chip	area	median counts/ pixel[a] (DN, total)	median counts/ pixel (DN, in 1800s)	Dark Current (e^- /sec/pixel)	ΔDN (total)
PC1	200:600,200:600	64.627	1.80	0.0071	1.18 1.8%
WF2	200:600,200:600	39.264	1.09	0.0043	1.95 4.8%
WF3	200:600,200:600	55.583	1.54	0.0059	4.51 7.7%
WF4	200:600,200:600	54.688	1.52	0.0060	1.19 2.2%
PC1	50:750,50:750	61.968	1.72	0.0068	
WF2	50:750,50:750	37.807	1.05	0.0042	
WF3	50:750,50:750	53.533	1.49	0.0057	
WF4	50:750,50:750	52.647	1.46	0.0058	
PC1	10:100,50:750	53.133	1.48	0.0058	
WF2	10:100,50:750	33.734	0.94	0.0037	
WF3	10:100,50:750	46.864	1.30	0.0050	
WF4	10:100,50:750	45.056	1.25	0.0049	

a. The data are from thirty-six 1800s darks in gain 7 taken between Oct. 04 - Nov. 08, 1999. The total exposure time is 64800s. The median counts/pixel in 1800s is given for comparison with the measurements of Baggett et al. (1998). The dark current is calculated using the gains in Table 4.3 of the WFPC2 Handbook.

Darks

The goal was to measure any changes in the darks to ~1.4 electrons/pixel (0.2 DN and 0.1 DN for gain 7 and 15 respectively). For the pre-SM3a data we extracted from the archive thirty-six 1800s darks taken under program 8442 in gain 7 between Oct, 04 - Nov, 08, 1999. We combined the darks using **crrej** to remove cosmic rays and determined the

median value in several regions, corresponding to (1) most of the chip, (2) the center 400x400 pixels and (3) the edge columns following Baggett et al. (1998). Results are given in Table 7.2 for the pre-SM3a darks. We also extracted thirty-six 1800s post-SM3a gain 7 darks from the period Jan. 11 to 31, 2000, from program 8491 and 8498 (post cool down). The results for the post-SM3a darks are given in Table 7.3. The data are consistent with an increase of a few percent (ranging from 2-8% depending on chip) in the dark current between October 1999 and January 2000. Figure 7.1 shows the dark current in DN/sec as a function of time from Jun. 1994 to Jan. 2000. Both pre- and post-SM3a points lie along the line of steadily increasing dark current found by Baggett et al. Thus, the post-SM3a results show only the expected gradual increase in dark current and there appears to be no effect of SM3a itself on the dark current.

Differences between pre- and post-SM3a darks show no significant structure in the central 400x400 pixels. A very small change (~ 3E-05 DN/s) is found in the row averages, but not in the column averages. Direct inspection shows that the variations are due to features in the pre-SM3a data which are not present in the post-SM3a data, i.e., the post-SM3a darks are “smoother”.

Table 7.3: Dark Current Post-SM3a, gain 7.

chip	area	median counts/ pixel[a] (DN, total)	median counts/ pixel (DN, in 1800s)	Dark Current (e-/sec/pixel)
PC1	200:600,200:600	65.806	1.83	0.0072
WF2	200:600,200:600	41.218	1.14	0.0045
WF3	200:600,200:600	60.097	1.67	0.0064
WF4	200:600,200:600	55.875	1.55	0.0061
PC1	50:750,50:750	62.952	1.75	0.0069
WF2	50:750,50:750	39.653	1.10	0.0044
WF3	50:750,50:750	57.982	1.61	0.0062
WF4	50:750,50:750	53.943	1.50	0.0059
PC1	10:100,50:750	53.815	1.49	0.0059
WF2	10:100,50:750	34.992	0.97	0.0038
WF3	10:100,50:750	50.447	1.40	0.0054
WF4	10:100,50:750	46.492	1.29	0.0051

a. The data are from thirty-six 1800s darks in gain 7 taken between Jan. 11 to Jan. 31, 2000 (post-SM3a and post cool down). Total exposure time is 64800s. The median counts/pixel in 1800s is given for comparison with the measurements of Baggett et al. (1998). The dark current is calculated using the gains in Table 4.3 of the WFPC2 Handbook.

Figure 7.1: Dark current (in DN/s) as a function of time from Jun. 1994 to Jan. 2000. The dark current is shown for three different regions: (1) most of the chip 50:750,50:750, (2) the chip center 200:600,200:600, and (3) the edge columns 10:100,50:750. The symbol key is +=PC, circle=WF2, cross=WF3, diamond=WF4.

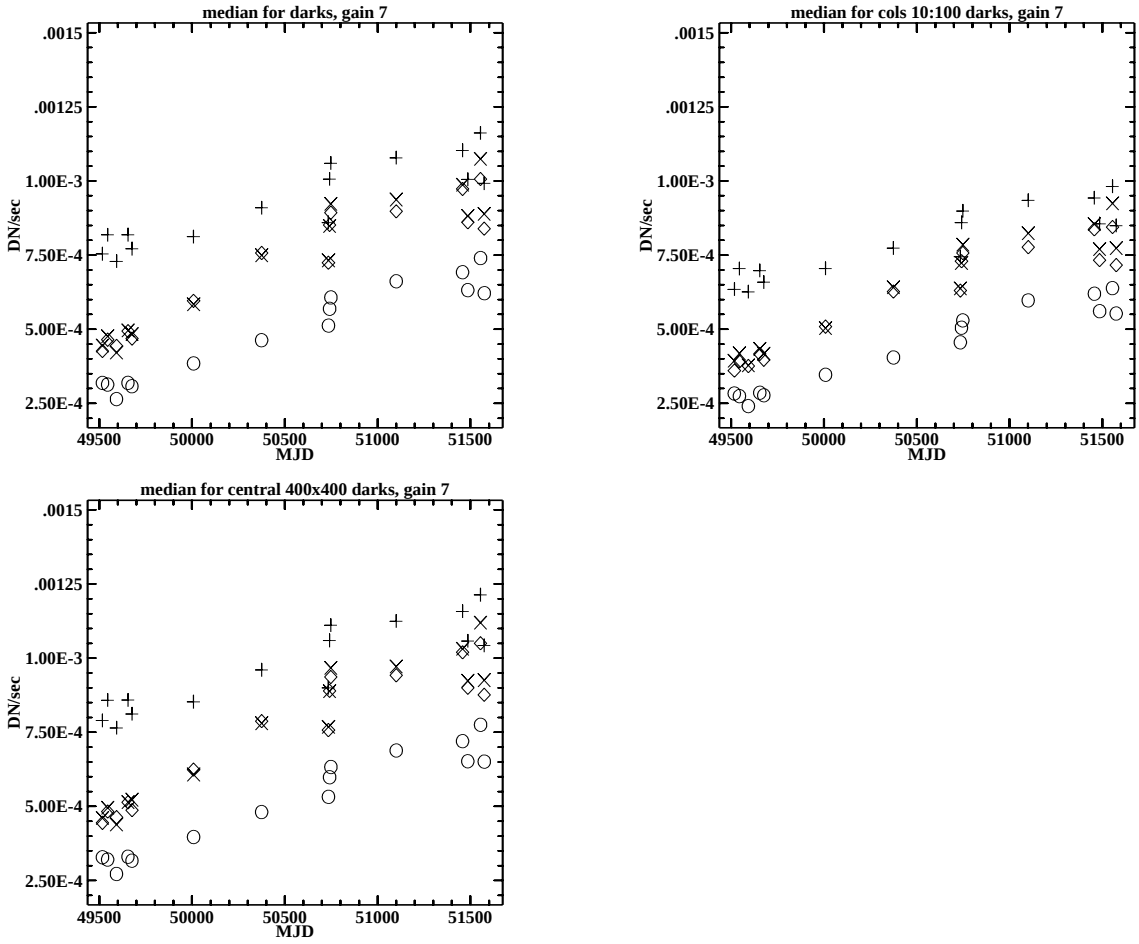

VISFLATs

The goal was to measure changes in the VISFLATs to ~ 1%. Due to the decline in the VISFLAT lamps with usage (Stiavelli & Baggett 1996), VISFLATs are now taken very rarely. There were sweeps though a set of filters in Mar. and Dec. 1998 and a sweep in Aug. 1999 in combination with polarizers. Thus the data from Dec. 98 were used as the pre-SM3a set. This consisted of pairs of observations in gain 7 from program 7623 in F439W, F555W, F675W, F814W, and one each in FR533N in both gains. The post-SM3a data set taken on Jan. 18, 2000, consisted of the same filter sweep plus F336W.

In order to check the stability of the flat fields and the lamp illumination, we combined the pairs of images at each filter using **crrej** and divided the Dec. 98 images by the Jan. 00 images. The statistics of the ratio images are given in Table 7.4. Due to the changes in the VISFLATs, the ratios averaged over the chips are not quite unity. The lamps have decreased in brightness by about 0.3% at F439W, 0.4% at F555W, 0.3% at F665W, and

have increased by 0.6% at F814W. The mean values of the images have a standard deviation of 1.6% and 0.8% for the PC and WF chips, respectively.

Table 7.4: Statistics of Ratios of Pre-/Post-SM3a VISFLAT Images.

chip	filter	median[a]	mean	stddev
PC1	F439W	1.0019	1.00221	0.01595
WF2	F439W	1.0028	1.00280	0.00747
WF3	F439W	1.0025	1.00254	0.00766
WF4	F439W	1.0026	1.00254	0.00775
PC1	F555W	1.0041	1.00444	0.01636
WF2	F555W	1.0043	1.00444	0.00764
WF3	F555W	1.0045	1.00458	0.00764
WF4	F555W	1.0050	1.00503	0.00776
PC1	F675W	1.0030	1.00324	0.01670
WF2	F675W	1.0027	1.00280	0.01670
WF3	F675W	1.0027	1.00278	0.00804
WF4	F675W	1.0028	1.00287	0.00792
PC1	F814W	0.9959	0.99619	0.01671
WF2	F814W	0.9933	0.99336	0.01671
WF3	F814W	0.9933	0.99344	0.01671
WF4	F814W	0.9930	0.99307	0.01671

a. Statistics of entire chip [50:750,50:750] of ratio images (pre-/post-SM3a data) for gain 7.

The ratio images themselves are smooth and featureless except for a positive/negative feature in WF4 at position 108, 787 with amplitude about 1 percent. This is likely to be due to a small movement of a dust speck on one of the optical surfaces. Similar changes in the past are reported by O'Dea et al 1999. Row and column averages of the ratio image vary by less than 0.05% rms. Thus, there are no significant changes in either the flat fields or the VISFLAT illumination pattern due to SM3a.

As a measurement of the gain ratio, we divided the FR533N gain 7 observation by the gain 15 exposure and determined the statistics of the inner 400x400 pixels. The results are given in Table 7.5, including also data from Mar. 1998 to provide a longer time baseline. The gain ratios increase by about 0.6% between Dec. 1998 and Jan. 2000, compared to 0.08% between Mar. and Dec. 1998. The long-term trend in gain ratios since 1994 is illustrated in Figure 7.2, which uses the MEANC300 value from the headers with the bias level subtracted. The ratio is relatively stable over time (though there is a downward trend seen in WF3). The jump seen in the last data point is larger than the typical point-to-point scat-

ter suggesting it is not due to noise. However, the ratios of gain 7 and 15 INTFLATs (see below) give an opposite direction for the jumps in the three WFC chips. If the change were due to an intrinsic change in the gain ratios, i.e., an actual change in the camera electronics, the variations would be consistent between VISFLAT and INTFLAT data. Because of the inconsistency, we suspect that the apparent change in gain ratios is actually due to changes in the lamps themselves - note that gain 7 and gain 15 images are taken at different points in the lamp cycle. Even if real, the change we see has a negligible impact on science observations.

Table 7.5: Stability of Gain Ratios

chip	date	median[a]	stddev	current/Dec-1998
PC1	Mar-07-98	0.98686	0.021	1.0006
WF2	Mar-07-98	0.99888	0.017	1.0010
WF3	Mar-07-98	1.00210	0.017	1.0011
WF4	Mar-07-98	1.00210	0.011	1.0007
PC1	Dec-08-98	0.98629	0.021	
WF2	Dec-08-98	0.99792	0.017	
WF3	Dec-08-98	1.00100	0.018	
WF4	Dec-08-98	0.97750	0.011	
PC1	Jan-18-00	0.99035	0.022	1.0041
WF2	Jan-18-00	1.00500	0.018	1.0071
WF3	Jan-18-00	1.00890	0.018	1.0079
WF4	Jan-18-00	0.98254	0.011	1.0051

a. Statistics of the FR5333N ratios (gain 7 60s exposure divided by gain 15 120s exposure). We present the median and the standard deviation of the mean value over the inner 400x400 pixels with a 10 σ clipping. The last column is the ratio of the median value for that date divided by the median on Dec. 08 1998.

We plot the ratio of the counts in the gain 7 and gain 15 FR533N images as a function of time from Mar. 1994 to Jan. 2000 in Figure 7.2. This uses the MEANC300 value from the headers with the bias level subtracted. The ratio is relatively stable over time (though there is a downward trend seen in WF3). The jump seen in the last data point is larger than the typical point-to-point scatter suggesting it is not due to noise. However, the ratios of gain 7 and 15 INTFLATs (see below) give an opposite direction for the jumps in the three WFC chips. If these were due to changes in the gain ratios, the jumps should be in the same directions in the VISFLAT and INTFLAT data. Thus, it appears that the jumps in the ratios may be due to changes in the brightness ratios of the lamps on short and long time scales.

Figure 7.2: Time dependence from Mar. 1994 to Jan. 2000 of the ratio of the gain 7 (60s exposures) divided by gain 15 (120s exposures) counts in FR533N VISFLAT images. Counts are determined from the MEANC300 header values with the bias levels subtracted. The dotted lines show the location of SM2 and SM3a. The gain 7 and 15 images were taken systematically back-to-back starting Aug. 1, 1995 (MJD 49930). Before that date they were taken on average several days apart. For dates prior to this, the ratio is obtained by using the two observations closest in time. However the lamp brightness does vary on these time scales resulting in larger scatter in the ratios of the earlier data. This figure supersedes Figure 10 of ISR WFPC2 99-01.

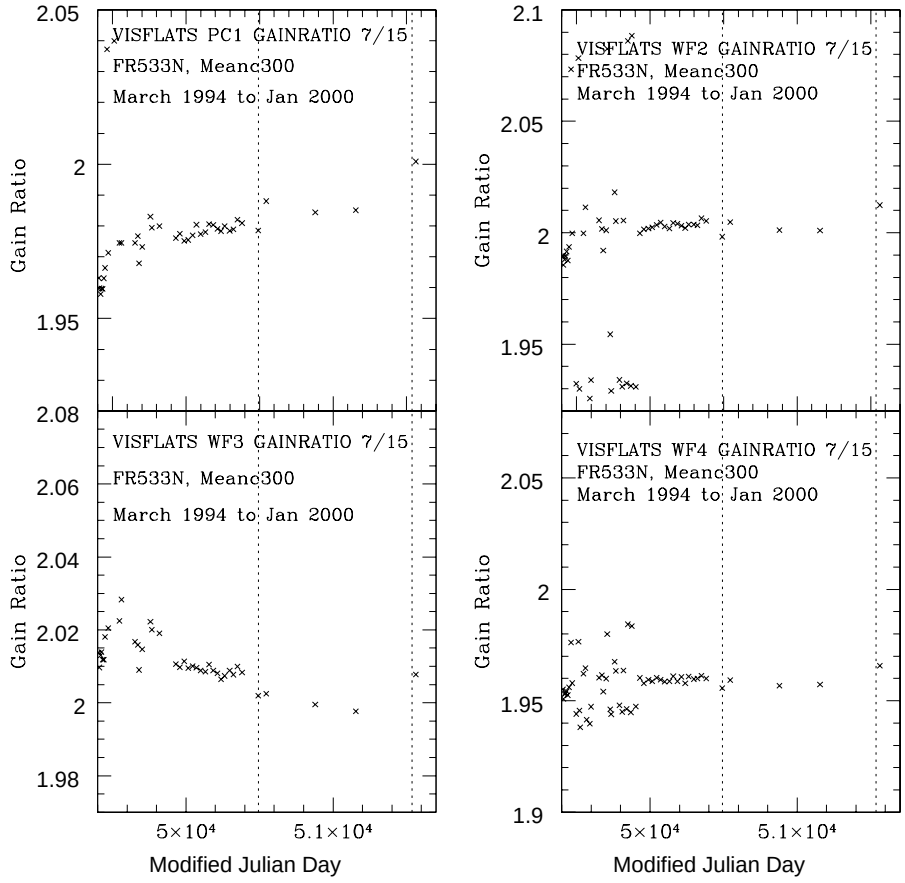

INTFLATs

The goal was to measure changes in the INTFLATs of about 1% accuracy. We created pre-SM3a master images in gain 7 for the filters F336W (four 1000s exposures), F555W (four 10s exposures) and F814W (four 1s exposures) by combining (with **crrej**) data taken in early and mid 1999. The post-SM3a masters are created using the same number of exposures taken in the period Jan.-Feb. 2000. We generated ratios of the post-SM3a master images with each of the earlier sets, and compared their statistics with the ratio of early to mid-1999 master images. The results are consistent with the INTFLAT brightness remaining constant for the three filters to within a few tenths of a percent over periods of about six months.

Figure 7.3: Average counts in the inner 300x300 of the F555W INTFLATs (10s exposures in gain 7 and 20s exposures in gain 15) determined using the MEANC300 header value and subtracting the average bias level value (from Table 2.4 of ISR WFPC2 97-04). The two servicing missions (SM2 and SM3a) are shown by the dotted lines. This plot supersedes Figure 1 of ISR WFPC2 99-01.

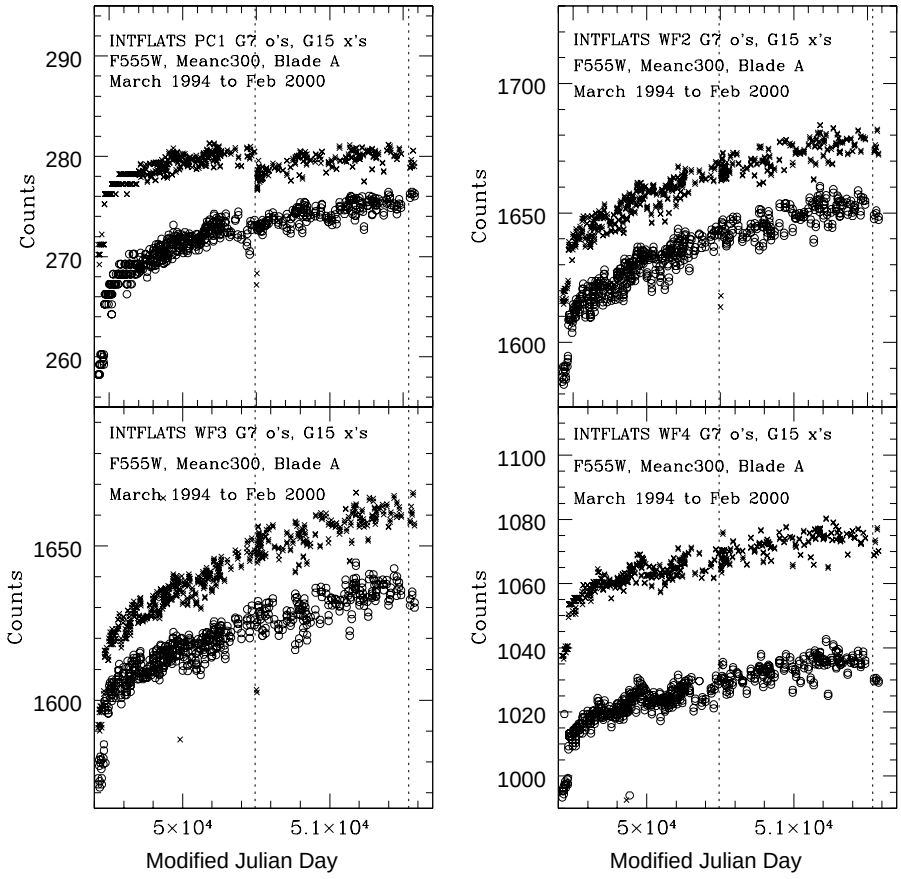

Figure 7.3 shows the average counts in the inner 300x300 of the F555W INTFLATs (10s exposures in gain 7 and 20s exposures in gain 15). As reported by O'Dea et al. (1999), there was a small jump in the counts in both gains in the PC1 INTFLATs at SM2. At SM3a, there are also small jumps (of order a few tenths of a percent) only in the gain 7 INTFLATs in all chips, with the largest changes being in PC1 and WF4. Although quite small, these changes at the level of a few tenths of a percent appear to be real since the changes are larger than typical scatter in the data. These changes are not likely to be due to a change in the sensitivity of the chips since the changes are not seen in gain 15. They do not seem likely to be due to changes in the gains since the changes are in opposite directions in PC1 and WF4, while the VISFLAT ratios of gain 7 and gain 15 images show changes in the same directions for both chips. The most likely explanation is that the jumps are due to the fact that the output of the bulbs is not steady at the few tenths of a percent level over time scales of 10-20s (see Figure 8d of O'Dea et al. 1999).

We consider next the information on gain ratios from the INTFLATs. The statistics of the ratio images (gain 7/gain 15) are given in Table 7.6 and Figure 7.4. In general the

ratios of INTFLAT count rates in the two gains are very steady, though in contrast to the biases and darks which show no effect, there have been small changes associated with the servicing missions. PC1 experienced a jump of 0.7% in the ratio at SM2 (see WFPC2 ISR 99-01); a jump of similar amplitude is seen after SM3a. WF2 is the most stable of the four chips with only a very gradual drift of order 0.1% over six years and negligible SM-related changes. WF3 shows a small downward drift until SM2, at which point there was a small downward jump, after which it is relatively stable. WF4 shows a small upward drift which is not affected by SM2, but there may have been a downward jump at SM3a due to a drop in the observed count rate (DN/s) in gain 7.

Table 7.6: Stability of INTFLAT F555W Gain 7 to Gain 15 Ratio.

chip	date	median[a]	stddev	current/Dec-1998
PC1	1999-09-15	1.9403	0.0248110	
WF2	1999-09-15	1.9695	0.0104700	
WF3	1999-09-15	1.9749	0.0106630	
WF4	1999-09-15	1.9263	0.0131000	
PC1	2000-01-15	1.9396	0.0221830	0.9996
WF2	2000-01-15	1.9659	0.0093314	0.9982
WF3	2000-01-15	1.9711	0.0094579	0.9981
WF4	2000-01-15	1.9213	0.0117880	0.9974

a. Statistics of images taken over the whole chip [50:750,50:750] of the ratio of INTFLAT F555W masters with gain 7 divided by gain 15. The ratio is normalized by the total exposure times for the master images. The last column is the ratio of the post-SM3a ratio divided by the pre-SM3a ratio.

We note that the general trends in the gain 7 and gain 15 ratios of observed count rates are similar in the VISFLATs and INTFLATs up through SM2, after which the two sets of data seem to diverge. However, VISFLATs are more poorly sampled after SM2. Since the VISFLATs and INTFLATs are independent systems, the trends suggest that from 1994 to 1997 there were small drifts and jumps in the gain of gain 7, however, after that the variations are dominated by variations in the lamps.

In order to determine the stability of the illumination pattern of the INTFLATs, we examined the images of the ratio of the Jan. 99, mid-99, and post-SM3a INTFLATs for F336W, F555W, and F814W. A greyscale representation of the ratio for F814W is shown in Figure 7.5, and row and column averages for F555W in WF4 are plotted in Figure 7.6. Large-scale variations are summarized in Table 7.7.

All three filters show large scale features in at least some chips with amplitude ranging from 0.1 to 1.0% with the smallest and largest variations in PC1 and WF4, respectively. The amplitude and structure of the variations are chip and wavelength dependent. The

largest variations occur in the corners and edges of the images, while the inner 400x400 regions are relatively more stable.

Figure 7.4: The ratio of the gain 7 and gain 15 count rates (DN/sec) determined from the MEANC300 header values corrected for the average bias levels. This figure supersedes Figure 9 of ISR WFPC2 99-01.

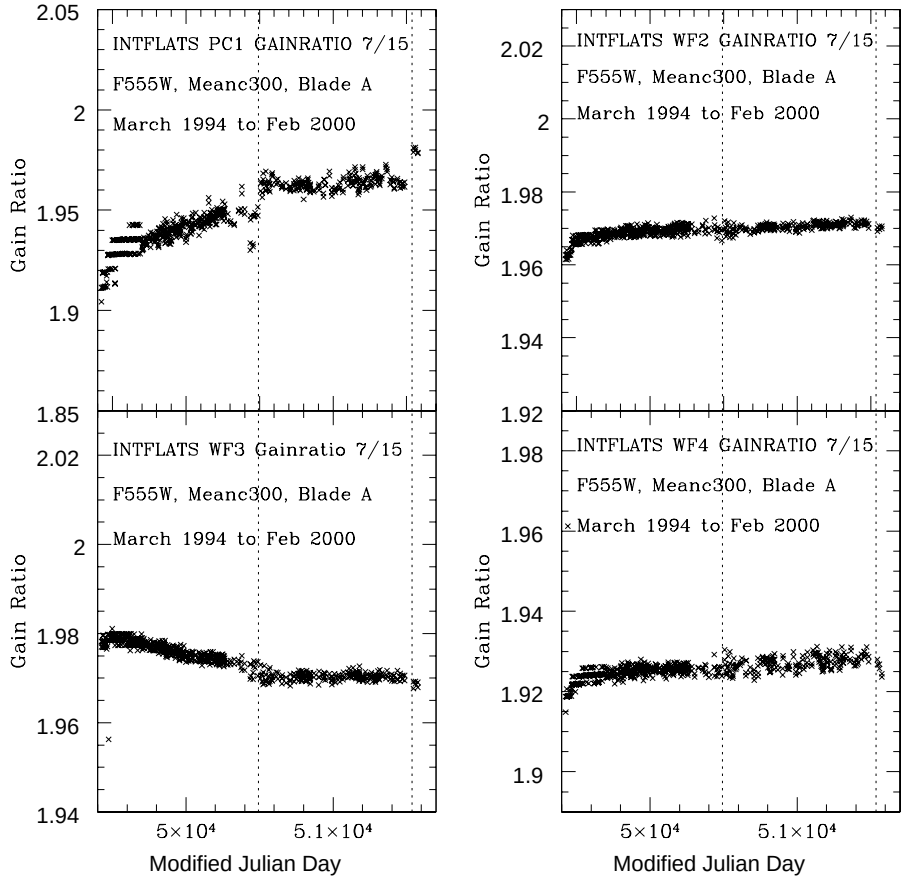

Table 7.7: Summary of Large Scale Variations in INTFLAT Ratios.

Region	F336W		F555W		F814W	
	jan99/ mid99[a]	**mid99/ jan00**	**jan99/ mid99**	**mid99/ jan00**	**jan99/ mid99**	**mid99/ jan00**
PC1 Rows	0.2%	0.1%	0.1%	0.25%	0.1%	0.15%
PC1 Columns	0.1%	0.1%	<0.1%	0.1%	0.1%	0.1%
PC1 Center Columns	<0.1%	<0.1%	<0.1%	0.1%	<0.1%	<0.1%
WF2 Rows	0.3%	0.15%	0.1%	0.3%	0.2%	0.3%
WF2 Columns	0.4%	0.4%	0.1%	0.7%	0.1%	0.1%
WF2 Center Columns	0.25%	0.2%	0.1%	0.4%	0.1%	<0.1%
WF3 Rows	0.7%	0.3%	0.4%	0.1%	0.1%	0.8%

Region	F336W		F555W		F814W	
WF3 Columns	0.6%	0.2%	0.4%	0.2%	0.2%	1.0%
WF3 Center Columns	0.4%	0.2%	0.15%	0.1%	0.1%	0.5%
WF4 Rows	0.1%	0.1%	0.1%	0.1%	0.1%	0.15%
WF4 Columns	1.1%	0.2%	0.7%	1.0%	0.5%	0.7%
WF4 Center Columns	0.7%	0.1%	0.5%	1.0%	0.45%	0.35%

a. Peak-to-peak amplitude of large scale variations in the INTFLAT illumination pattern over roughly six month intervals. These measurements ignore the edges of the chips which can have larger variations.

These changes in the illumination pattern are likely caused by the fact that the four Carley bulbs do not vary in the same manner. The fact that the changes are wavelength dependent suggests that the changes in brightness are associated with changes in temperature.

These results have implications for the use of INTFLATs for pre-flashing to reduce CTE. The master INTFLAT which is used to subtract the signature of the INTFLAT from the background should be constructed of INTFLATs taken close to the observation - determination of the exact time period requires further study.

Figure 7.5: Ratio of INTFLAT gain 7 image in F814W taken pre-SM3a (May-Nov. 99) and post-SM3a (Jan.-Feb. 00). The display grey-scale ranges from 0.97 (black) to 1.02 (white).

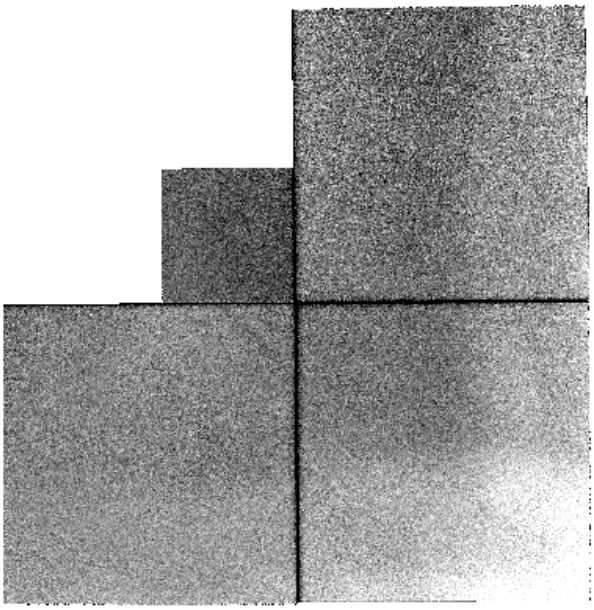

Figure 7.6: Row and column plot of the ratio of Jan 2000 to mid-1999 INTFLATs in F555W.

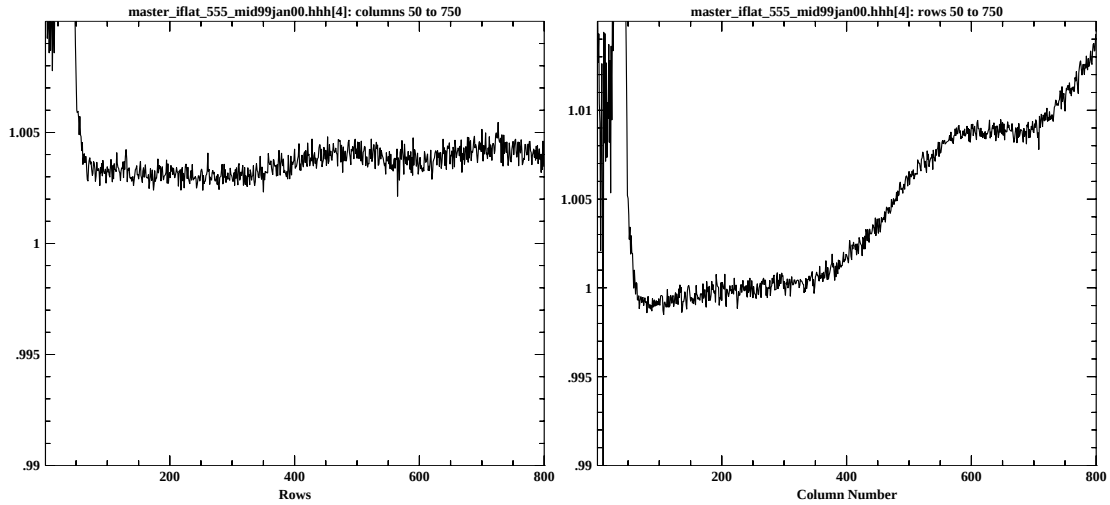

K-SPOTS

The goal was to measure relative shifts of the K-spots to an accuracy of 0.1 pixel (1-sigma). We determined the initial location of the K-spots by displaying the images and using **imexamine** to estimate the positions. The positions were then put into a file which were used as input to the IRAF task **center**, which was run on the K-spot images using the centroid algorithm with a box width of 3 pixels. We used exposures of the 2.6s and 1s for PC1 and the WF chips, respectively. There were 11 and 24 usable K-spots in the PC and WF chips, respectively.

The difference between the measured K-spot locations in the images of Nov. 2 and 3, 1999, was used as a baseline to indicate the expected scatter in the measurements. The differences, in the sense (early date - late date), are plotted in Figure 7.7; their averages are given in Table 7.8.

Figure 7.7 shows that the shifts for each chip are displaced from zero by a few mas with a scatter of a few mas. The values for each chip tend to clump together, without much overlap between chips. This suggests that either, (1) there are real apparent movements of the K-spots on one chip relative to another of a few mas on a one day time scale, or (2) there are systematic chip-dependent errors in determining shifts of the K-spots.

The data spanning SM3a -- Nov. 3, 1999, to Jan. 11, 2000 -- show shifts several times larger than the Nov. 2 to 3 shifts (Figure 7.8). Thus, there were real shifts in the K-spot locations over this time period. These shifts are generally consistent with the trend in the K-spot shifts found by MS97. However, historically, PC1 has had the largest shifts, whereas in this time period, WF3 has shifted the most. Thus, the slope of the shifts appears to be changing.

Table 7.8: Average K-spot Shifts.

chip	date 1	date 2	avg x shift[a]	rms	avg y shift	rms
PC1	11-02-99	11-03-99	0.720	0.776	6.424	2.150
WF2	11-02-99	11-03-99	1.059	4.518	-2.164	7.302
WF3	11-02-99	11-03-99	-1.286	2.117	-3.576	1.256
WF4	11-02-99	11-03-99	-4.002	2.863	-0.653	3.501
PC1	11-03-99	01-11-00	-1.572	0.991	-6.304	1.987
WF2	11-03-99	01-11-00	-7.796	1.899	-5.007	2.689
WF3	11-03-99	01-11-00	-10.377	6.052	-8.973	4.026
WF4	11-03-99	01-11-00	-9.598	4.475	-3.957	1.720

a. Average differences in x and y shifts (in milliarcsec) for each chip. The differences are in the sense (early date - later date).

Figure 7.7: Differences in the locations of the Kelsall spots between Nov. 2 and Nov. 3, 1999, in the sense (early date - later date).

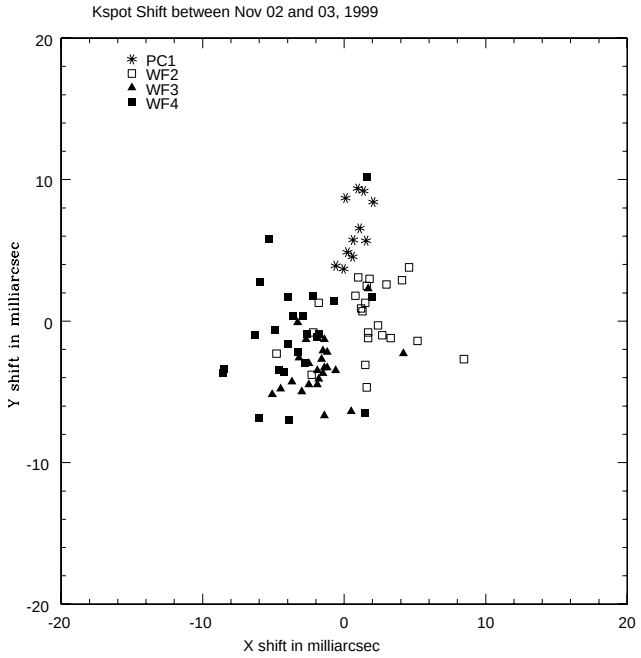

Figure 7.8: Differences in the locations of the Kelsall spots over the period spanning SM3a - Nov. 3, 1999, to Jan. 11, 2000, in the sense (early date - later date).

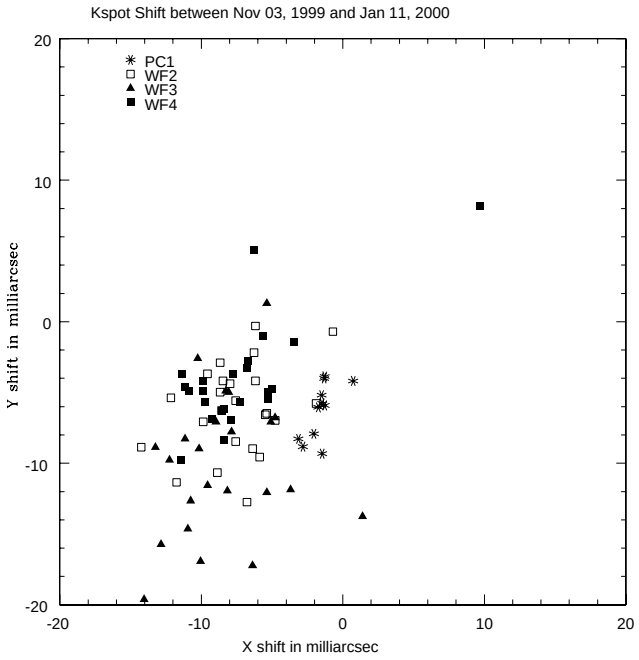

Conclusions

We have studied the stability of WFPC2 with special attention to any potential changes due to SM3a as determined from internal calibration observations. Over the course of the period Nov. 1999 to Jan. 2000, there were no significant changes in the gain 7 or 15 read noise.

The data from the dark images are consistent with an increase of a few percent (ranging from 2-8% depending on chip) in the dark current between October 1999 and January 2000. The data show that the pre- and post-SM3a points lie along the line of steadily increasing dark current found by Baggett et al. Thus, the post-SM3a results show only the expected gradual increase in dark current and there appears to be no effect of SM3a itself on the dark current.

Ratios of VISFLATs taken Dec. 1998 and Jan. 2000 show that there are no substantial changes in either the flat fields or the VISFLAT illumination pattern due to SM3a. The ratio of gain 7 and gain 15 VISFLATs does show a small increase of order 0.5 percent between Dec. 1998 and Jan. 2000. This may correspond to a change in the gain ratios or to the ratios of VISFLAT lamp brightness over 60 and 120 sec intervals.

We note that the general trends in the gain 7 and gain 15 ratios of observed count-rates are similar in the VISFLATs and INTFLATs up through SM2, after which the two sets of data seem to diverge. However, the VISFLAT data are more poorly sampled after SM2.

Since the VISFLATs and INTFLATs are independent systems, the trends suggest that from 1994 to 1997 there were small drifts and jumps in the gain of gain 7, however, after that the variations in the ratios are dominated by variations in the lamps.

There have been small (few tenths of a percent) changes in the INTFLAT lamp brightness in gain 7 associated with both servicing missions (but not in gain 15 except for the PC1 at SM2). We see changes in the illumination pattern of the INTFLATs associated with the changes in intensity. Ratios of INTFLATs taken in mid-99 and Jan 2000 show small amplitude (0.1 - 1%) large scale variations which are chip and wavelength dependent. These variations are somewhat larger than those seen in a similar time interval from Jan 99 to mid-99. We suggest that the four Carley bulbs are not varying in the same manner and that this induces the observed changes in the illumination pattern of the INTFLATs. The variation in the lamp brightness may be associated with changes in temperature.

Over the period Nov. 3, 1999 to Jan. 11, 2000 the Kelsall spots shifted by on average 10 milliarcsec. These shifts are consistent with the known time evolution of the K-spot positions.

In summary, overall the WFPC2 appears to be very stable exhibiting only the minor changes expected due to known low level variability. The only variations attributable to SM3a are small changes in INTFLAT lamp brightness.

Acknowledgements

We are grateful to Stefano Casertano for helpful discussions and to John Biretta for comments on an early version of the manuscript.

References

Baggett, S., Casertano, S., & Wiggs, M. S., 1998, TIR WFPC2 98-03

Mutchler, M. & Stiavelli, M., 1997, TIR WFPC2 97-07

O’Dea, C. P., Gonzaga, S., McMaster, M., Heyer, I., Hsu, J. C., Baggett, S., Rudloff, K., 1997, ISR WFPC2 97-04

O’Dea, C., Mutchler, M., & Wiggs, M., 1999, ISR WFPC2 99-01

8: SMOV3a Flat Field Stability Check

by Anton M. Koekemoer, John Biretta and Michael S. Wiggs

Summary: We compare WFPC2 Earthflats taken before and after the 1999 service mission 3a. Most of the field-of-view shows no change (<0.3%) in flat field calibration. The largest changes occur only near the CCD corners, particularly near the apex, and reach

~1.5%; these are likely attributable to long-term changes in the camera geometry, rather than SM3a.
Note: these results have been reported independently as WFPC2 Technical Instrument Report (TIR) 00-01, *SMOV3a Flat Field Stability Check*, by Anton M. Koekemoer, John Biretta and Michael S. Wiggs.

Introduction

As part of our post-servicing check-out of WFPC2 after SM3a, we have examined a series of F502N Earthflats to test the flat field stability. The goal of these observations is to test for any unexpected OTA obscuration or contamination in WFPC2 that may have occurred as a result of the servicing mission. The flats are also capable of revealing changes in the OTA / WFPC2 geometry, as well as any QE changes localized to one CCD camera or to a small region of the field-of-view. While internal flats can provide some of this information, the Earthflats are unique in providing an end-to-end test of the OTA+WFPC2 system. Detailed discussion of Earthflats and WFPC2 flat fields can be found elsewhere (Biretta 1995).

Observations and Analyses

Earthflats were observed as part of the routine calibration proposals 8053 and 8445 for late Cycle 7 and Cycle 8, as well as proposal 8495 during SMOV3a. All the F502N flats are 1.2 second exposures of the bright Earth made with gain 15. Since we are interested primarily in changes to the flat field, we select subsets of these to construct a pre-SMOV and an SMOV flat.

For the pre-SMOV observations we started with a total of 174 Earthflats in F502N taken between March 1999 and July 1999 as part of proposals 8053 and 8445. We discarded images with mean counts in the PC1 below 600 DN and mean counts in the three WFC chips above 3200 (to avoid saturation), leaving a total of 48 images. These images were then examined for streaks (produced by features on the Earth moving across the detector), after multiplying with the current F502N flat field reference file. The streaks increase the overall RMS of the image; displaying the images and examining them with **imstat** allowed the rejection of images with prominent streaks (more than around 0.8% overall normalized RMS, and exceeding about 1% peak-to-peak amplitude). Images with prominent “worms” in WF2 were also rejected. The remaining eight images, u59m1l03r, u59m2n04r, u59m2x04r, u59m3i03r, u59m3q04r, u59m4q04r, u59m4s03r, and u59m7104r, were combined with the task **streakflat** to produce an averaged, de-streaked pre-SMOV flat.

The same rejection criteria were applied to the 44 Earthflats taken after the service mission as part of programs 8445 and 8495. Again the images were displayed and examined with IMSTAT, rejecting those with too high an RMS and large peak-to-peak streak

variations. All the flats from program 8495 had to be discarded, either because of low flux or saturation, or unacceptable streak variations. The remaining five acceptable images were all from program 8445, taken during Feb 16 - 21, 2000. These images, u5jf3i04r, u5jf3k03r, u5jf3m03m, u5jf3o04r, and u5jf3p04r, were combined with STREAKFLAT to produce the SMOV flat.

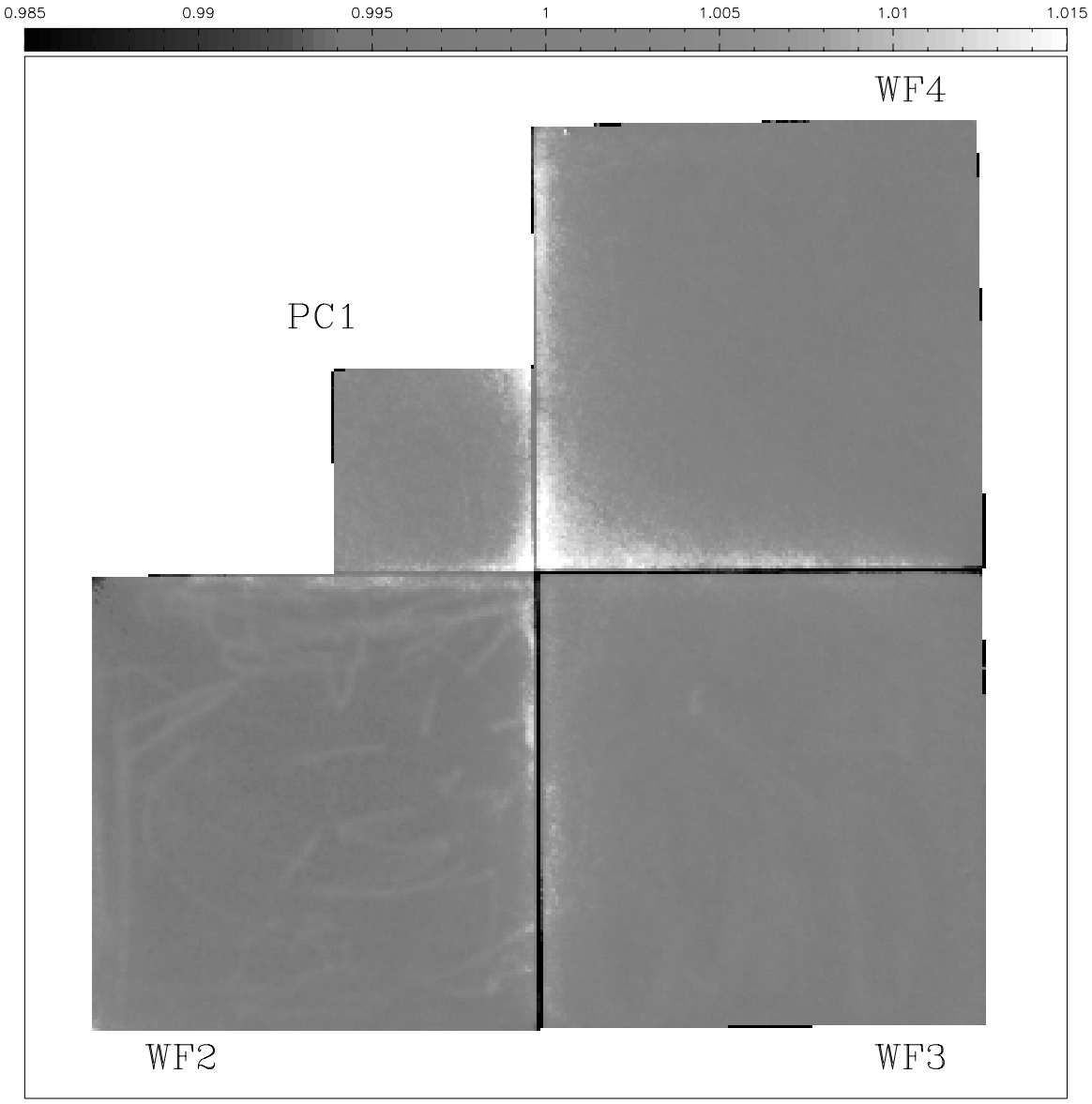

Figure 8.1: Ratio of SMOV / pre-SMOV flats taken in F502N. The display greyscale ranges from 0.985 (black) to 1.015 (white). The label of each WFPC2 chip is indicated in the figure. For display purposes the original 1600 x 1600 pixel image has been median-smoothed and averaged using a 5x5 pixel box.

We then divided the SMOV flat by the pre-SMOV image, and normalized so that the central 400x400 pixels of WF3 had a mean of unity. The resulting SMOV / pre-SMOV ratio image is shown in Figure 8.1.

Results

Figure 8.1 shows that the mean ratio between the pre- and post-servicing flats is essentially unity. The most significant changes are seen in the corners of PC1 and WF4 near the pyramid apex, where departures from unity reach about 1.5% within about 10 pixels of the apex. These effects in the CCD corners are most likely due to small changes in the camera vignetting, which in turn result from small changes in the geometry of WFPC2. Other evidence of such small on-going geometric changes is also seen in K-spot images and is described by Mutchler and Stiavelli (1997) and in Section 4, K-spots, .

There is also slight evidence of the “worm” features on WF2 at low levels (0.2% peak-to-peak), related to contamination on the CCD windows. This is to be expected, since our only acceptable post-SMOV Earthflats were several weeks after decontamination.

The pixel-to-pixel fluctuations (over the central 400 x 400 pixels) in the ratio image are typically 0.4% RMS for the WFC CCDs, and 0.8% RMS for PC1, which is entirely consistent with photon statistical noise. After smoothing with a 10-pixel FWHM Gaussian function, the fluctuations decrease to <0.1% RMS, as would be expected for photon noise.

No change in chip-to-chip sensitivity is seen in on any levels above ~0.3% in the average ratio of post-SMOV / pre-SMOV counts over the central 400x400 pixels of each CCD. There is also no significant evidence of obscuration or other changes in the OTA.

References

Biretta, J., “WFPC2 Flat Field Calibration,” in Calibrating HST: Post Servicing Mission, eds. A. Koratkar and C. Leitherer, STScI, p. 257, 1995.

Mutchler, M. and Stiavelli, M. “WFPC2 Internal Monitoring for SM97,” Technical Instrument Report WFPC2-97-07.